An efficient reduced-order method with PGD for solving journal bearing hydrodynamic lubrication problems

Bilal Cherabi [a,*], Abderrachid Hamrani [a], Idir Belaidi [a], Sofiane Khelladi [b], Farid Bakir [b]

[a] Research team MISP, LEMI, Université M'hamed-Bougara Boumerdès (UMBB), 35000, Boumerdès, Algeria
[b] Arts et Métiers ParisTech, DynFluid, 151, boulevard de l'Hôpital, 75013 Paris, France

B S T R A C T

In the present work, a reduced-order method, "Proper Generalized Decomposition (PGD)" is extended and applied to the resolution of the Reynolds equation describing the behavior of the lubricant in hydrodynamic journal bearing. The PGD model is employed to solve the characteristic 'Reynolds' partial differential equation using the separation technique through the alternating direction strategy. The resulting separated-dimension system has a low computation cost compared to classical finite-difference resolution. Several numerical benchmark examples are investigated to verify the validity and accuracy of the proposed method. It has been found that numerical results obtained by the PGD method can achieve an improved convergence rate with a very low computation cost.

1. Introduction

The fundamental basis of hydrodynamic lubrication theory was firstly developed by O. Reynolds in 1886 [1]. Reynolds' analysis was inspired by previous experimental findings of N.P. Petrov [2] and B. Tower [3], who demonstrated that the viscosity is the most important property in film lubrication and that the load-carrying ability of a bearing is the result of the high pressures developed in the clearance space between the journal and the sleeve [4]. The so-called "Reynolds equation" provides essentially a prediction of the pressure distribution in the thin film lubrication, which is derived from the Navier–Stokes and continuity equations for incompressible flows [5]. Several approaches have been proposed to solve the Reynolds partial differential equation describing the journal bearing lubrication behavior. On one side, we can find the analytical models, which under certain conditions and simplifications can give some interesting results for very particular cases (infinitely short bearing [6,7], infinitely long bearing [8], finite bearing [9,10]). On the other side, several numerical methods have been developed to solve the fluid film lubrication problems; Raimondi and Boyd [11] applied the finite-difference method in the design and analysis of finite journal bearings. In general, journal bearing lubrication problems were solved using the finite element method in [12]. Deligant et al. [13] have solved the Reynolds equation by a finite-difference method using the Gauss–Seidel iterative method. Liang et al. [14,15] have used FDM (Finite Difference Method) in the study of hydrodynamic journal bearing. These methods are known to be accurate, but very time consuming [16], which motivates the search for new approaches with considerably lower computational cost [17]. Model reduction methods have gained a lot of

* Corresponding author.
E-mail address: bilal.cherabi@gmail.com (B. Cherabi).

interest in the last decade [18,19]. In the field of fluid mechanics, the a posteriori model reduction method named Proper Orthogonal Decomposition (POD) has been widely used to simulate computational fluid problems [20–22]. Note that this method requires the snapshot of the flow issued from higher fidelity methods, which is often related to a significant computational cost. This drawback is circumvented in the a priori methods, where the reduced model is constructed without prior knowledge of the solution. The LATIN method, considered to be the first a priory model reduction method, was proposed by P. Ladeveze [23]. This method established a separated representation of the space and time coordinates for a complex physical model. It have been adopted to multi-physics frameworks [24–26]. In the case of complex fluids descriptions, a generalized representation was employed by [27–29] for approximating the solution to multi-dimensional characteristic partial differential equations. Dumon et al. [30] demonstrated the ability of PGD (Proper Generalized Decomposition) to solve many classical fluid problems accurately with considerable computational time saving. In [31], PGD was coupled with spectral discretization to solve several transfer and Navier–Stokes equations. Aghighi et al. [32] applied PGD to solve the Rayleigh–Bénard flow problem that studies the natural thermal convection. Tamellini et al. [33] proposed a method for solving the steady incompressible Navier–Stokes equation based on PGD coupled with stochastic Galerkin approximation.

In our work, the first of its kind, the extension of the Proper Generalized Decomposition (PGD) approach to the resolution of the hydrodynamic lubrication problems in journal bearing is proposed, with the objective of reducing the computational cost of the simulation. In this paper, the PGD method is formulated and applied to the steady hydrodynamic lubrication equation. Section 2 describes the governing equations for hydrodynamic journal bearing, section 3 details the separated representation of the Reynolds equation with the use of the alternating direction strategy scheme and its PGD implementation, section 4 presents the numerical results obtained by PGD for the solution to the Reynolds equation. Comparisons are made with other classical methods through several benchmark examples. Finally section 5 concludes the work.

2. Governing equations for hydrodynamic journal bearing

2.1. Reynolds equation

The Reynolds equation in the hydrodynamic lubrication describes the pressure distribution in journal bearing, which is an elliptic, partial and differential equation for the pressure in terms of lubricant properties, density and viscosity, as well as the film thickness under simplifying assumptions [34]. For a Newtonian fluid, the Reynolds equation is written as

$$\frac{\partial}{\partial x}\left(h^3\frac{\partial P}{\partial x}\right)+\frac{\partial P}{\partial z}\left(h^3\frac{\partial P}{\partial z}\right)=6\mu R_a\omega\frac{\mathrm{d}h}{\mathrm{d}x} \tag{1}$$

We can express the Reynolds equation (1) in the θ and z coordinates by the following development:

$$\frac{\partial h^3}{\partial x}\frac{\partial P}{\partial x}+h^3\frac{\partial^2 P}{\partial x^2}+h^3\frac{\partial^2 P}{\partial z^2}=6\mu R_a\omega\frac{\mathrm{d}h}{\mathrm{d}x} \tag{2}$$

so

$$3h^2\frac{\mathrm{d}h}{\mathrm{d}x}\frac{\partial P}{\partial x}+h^3\frac{\partial^2 P}{\partial x^2}+h^3\frac{\partial^2 P}{\partial z^2}=6\mu R_a\omega\frac{\mathrm{d}h}{\mathrm{d}x} \tag{3}$$

We make the following transformations:

$$\begin{cases}\mathrm{d}x=R_a\cdot\mathrm{d}\theta\\ \partial x=R_a\cdot\partial\theta\end{cases} \tag{4}$$

so the previous equation (3) becomes:

$$\frac{3h^2}{R_a^2}\frac{\mathrm{d}h}{\mathrm{d}\theta}\frac{\partial P}{\partial\theta}+\frac{h^3}{R_a^2}\frac{\partial^2 P}{\partial\theta^2}+h^3\frac{\partial^2 P}{\partial z^2}=6\mu\omega\frac{\mathrm{d}h}{\mathrm{d}\theta} \tag{5}$$

then the Reynolds equation with the θ and z coordinates Fig. 1 is written as

$$\frac{3}{hR_a^2}\frac{\mathrm{d}h}{\mathrm{d}\theta}\frac{\partial P}{\partial\theta}+\frac{1}{R_a^2}\frac{\partial^2 P}{\partial\theta^2}+\frac{\partial^2 P}{\partial z^2}=6\frac{\mu\omega}{h^3}\frac{\mathrm{d}h}{\mathrm{d}\theta} \tag{6}$$

where P is the pressure, h is the film thickness, R_a is the bearing radius, ω is the angular velocity and μ is the lubricant's viscosity.

The oil film thickness, h, which in turn varies as a function of the angular position θ, is calculated from the following equation

$$h=C(1+\epsilon\cos\theta) \tag{7}$$

where $\epsilon=\frac{e}{C}$ is the eccentricity ratio, e is the eccentricity, C is the radial clearance.

The pressure is influenced by the geometry of the fluid wedge, which is formed to sustain the load, as illustrated in Fig. 1 [4].

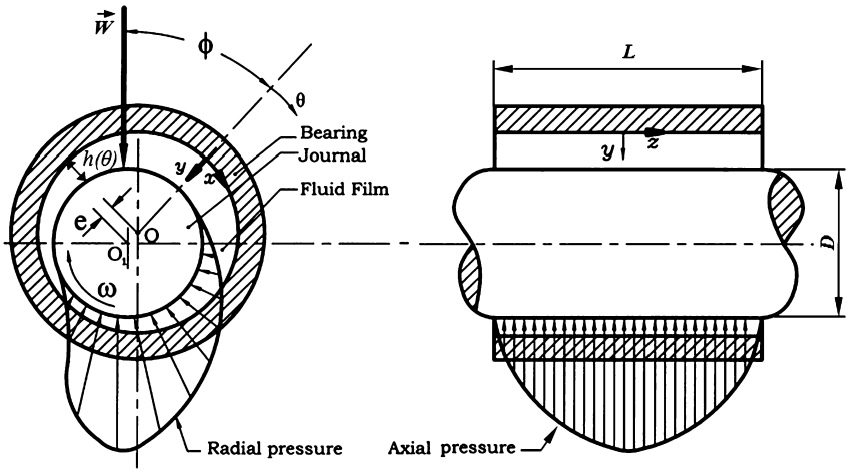

Fig. 1. Journal bearing-geometric parameterization.

2.2. Journal bearing characteristics

2.2.1. Load applied to the shaft

The integral of the pressure distribution obtained from the Reynolds equation should balance the externally applied load W, in order to have an equilibrium of forces. For the two-dimensional problem, this condition reads:

$$W = \int_0^{2\pi} \int_{-L/2}^{+L/2} P(\theta, z)\, \mathrm{d}\theta \mathrm{d}z \tag{8}$$

with

$$W = \sqrt{W_x^2 + W_y^2} \tag{9}$$

where the load components are written as:

$$\begin{cases} W_x = \int_0^{2\pi} \int_{-L/2}^{+L/2} P(\theta, z) \cos\theta \, R \, \mathrm{d}\theta \mathrm{d}z \\ W_y = \int_0^{2\pi} \int_{-L/2}^{+L/2} P(\theta, z) \sin\theta \, R \, \mathrm{d}\theta \mathrm{d}z \end{cases} \tag{10}$$

2.2.2. Sommerfeld number

The characteristics in steady running of a journal bearing of specified design are usually expressed non-dimensionally as functions of a single parameter called the Sommerfeld Number [35]. It is often referred to as the bearing characteristic number. The Sommerfeld number, S, has been conveniently used to compare the various non-dimensional characteristics of varied bearing arcs. The Sommerfeld Number can be mathematical represented as in equation (11):

$$S = \frac{\mu L D N}{W} \left(\frac{R}{C}\right)^2 \tag{11}$$

where L is the bearing length, D the shaft diameter, N the rotational speed of the shaft.

2.2.3. Friction torque

The friction torque is obtained by integrating the shear stresses acting on the journal:

$$C_{\mathrm{fr}} = \int_0^{2\pi} \int_{-L/2}^{+L/2} R \left(\mu \frac{\partial P}{\partial \theta} (2z - h) + R\omega \frac{\mu}{h} \right) \mathrm{d}\theta \mathrm{d}z \tag{12}$$

and the friction number is defined as follows:

$$f = \frac{C_{\mathrm{fr}}}{C \cdot W} \tag{13}$$

2.3. Analytical solution in particular cases

We can solve the Reynolds equation analytically by introducing a geometrical simplification corresponding to the infinitely short/long bearing.

2.3.1. Infinitely short journal bearing

When the ratio L/D is small, the circumferential pressure gradient can be neglected in comparison with the axial pressure gradient. This assumption was made for the first time by Michell [7] and developed by Ocvirk and Dubois [6]. It is justified for bearings with L/D smaller or equal to 1/8. Practically, this assumption is used for L/D up to 0.5 since the errors remain small on torque and flow rate and remain acceptable for the load-carrying capacity. Errors become very important for the maximum pressure in the film. They decrease with eccentricity. The Reynolds equation can then be written as:

$$\frac{\partial}{\partial z}\left(h^3\frac{\partial p}{\partial z}\right)=6\mu\omega\frac{\mathrm{d}h}{\mathrm{d}\theta} \tag{14}$$

with the boundary conditions:

$$\begin{aligned} &P\left(\theta, z=-\tfrac{L}{2}\right)=0\\ &P\left(\theta, z=+\tfrac{L}{2}\right)=0 \end{aligned} \tag{15}$$

The pressure field is:

$$P(\theta,z)=-\frac{3\mu\omega}{C^2}\left(z^2-\frac{L^2}{4}\right)\frac{\epsilon\,\sin\theta}{(1+\epsilon\cos\theta)^3} \tag{16}$$

The pressure varies as $\sin\theta$; it is positive for $\theta\in[0,\pi]$. To assess the load, Ocvirk and Dubois used Gtimbel's boundary conditions:

$$W=\mu LR\omega\left(\frac{L}{D}\right)^2\left(\frac{R}{C}\right)^2\frac{\varepsilon}{\left(1-\varepsilon^2\right)^2}\sqrt{16\varepsilon^2+\pi^2\left(1-\varepsilon^2\right)} \tag{17}$$

Sommerfeld's number is:

$$S=\left(\frac{D}{L}\right)^2\frac{\left(1-\varepsilon^2\right)^2}{\pi\varepsilon\sqrt{16\varepsilon^2+\pi^2\left(1-\varepsilon^2\right)}} \tag{18}$$

The friction torque is given by:

$$C_\mathrm{a}=\frac{\mu\omega R^3L}{C}\frac{\pi\,(2+\varepsilon)}{(1+\varepsilon)\sqrt{1-\varepsilon^2}} \tag{19}$$

and the journal friction number:

$$f=\frac{C_\mathrm{a}}{CW}=\frac{\pi^2S\,(2+\varepsilon)}{(1+\varepsilon)\sqrt{1-\varepsilon^2}} \tag{20}$$

The axial flow rate is:

$$Q_z=LCV\varepsilon \tag{21}$$

2.3.2. Infinitely long journal bearing

In the approximation of an infinitely long bearing, the axial flow is neglected with respect to the circumferential one. This assumption is used for L/D ratios up to 4. Then the Reynolds equation (6) is reduced to:

$$\frac{3}{hR_\mathrm{a}^2}\frac{\mathrm{d}h}{\mathrm{d}\theta}\frac{\partial P}{\partial\theta}+\frac{1}{R_\mathrm{a}^2}\frac{\partial^2P}{\partial\theta^2}=6\frac{\mu\omega}{h^3}\frac{\mathrm{d}h}{\mathrm{d}\theta} \tag{22}$$

with the Reynolds boundary conditions:
$P(\theta=0)=0$ or $P(\psi=0)=0$
$P(\theta=0_\mathrm{s})=\left(\frac{dP}{d\theta}\right)_{\theta=\theta_\mathrm{s}}=0$ or $P(\psi=\psi_\mathrm{s})=\left(\frac{dP}{d\psi}\right)_{\psi=\psi_\mathrm{s}}=0$
and the change in the variable of Sommerfeld [36]:

$$1+\varepsilon\cos\theta=\frac{1-\varepsilon^2}{1-\varepsilon\cos\psi} \tag{23}$$

The pressure field is given by:

$$P(\psi) = \frac{6\mu R^2 \omega}{C^2\left(1-\varepsilon^2\right)^{3/2}}\left\{\psi - \varepsilon\sin\psi - \frac{2\psi - 4\varepsilon\sin\psi + \varepsilon^2\psi + \varepsilon^2\sin\psi\cos\psi}{2(1-\varepsilon\cos\psi_s)}\right\} + P_a \tag{24}$$

where ψ_s corresponds to the abscissa of film break down location, and is defined by:

$$\varepsilon\left(\sin\psi_s\cos\psi_s - \psi_s\right) + 2\left(\sin\psi_s - \psi_s\cos\psi_s\right) = 0 \tag{25}$$

The load is given by the flowing equation:

$$W = 3\mu R\omega L\left(\frac{R}{C}\right)^2 \frac{1}{\sqrt{1-\varepsilon^2}(1-\varepsilon\cos\psi_s)}\sqrt{\frac{\varepsilon^2(1-\cos\psi_s)^4}{1-\varepsilon} + 4(\sin\psi_s - \psi_s\cos\psi_s)^2} \tag{26}$$

the attitude angle by:

$$\mathrm{tg}\,\phi = \frac{2\sqrt{1-\varepsilon^2}\left(\sin\psi_s - \psi_s\cos\psi_s\right)}{\varepsilon(1-\varepsilon\cos\psi_s)^2} \tag{27}$$

the Sommerfeld's number by:

$$S = \frac{\sqrt{1-\varepsilon^2}(1-\varepsilon\cos\psi_s)}{3\pi\sqrt{\frac{\varepsilon^2(1-\varepsilon\cos\psi_s)^4}{1-\varepsilon^2} + 4(\sin\psi_s - \psi_s\cos\psi_s)^2}} \tag{28}$$

the friction torque by:

$$C_a = \frac{\mu R^3\omega L}{C}\left[\frac{2\pi + \varepsilon\left(\sin\psi_s - \psi_s\cos\psi_s\right)}{\sqrt{1-\varepsilon^2}(1-\varepsilon\cos\psi_s)}\right] + \frac{e}{2}W\sin\phi \tag{29}$$

the journal friction number by:

$$f = \frac{C_a}{CW} = \pi S\left[\frac{2\pi + \varepsilon\left(\sin\psi_s - \psi_s\cos\psi_s\right)}{\sqrt{1-\varepsilon^2}(1-\varepsilon\cos\psi_s)}\right] + \frac{\varepsilon}{2}\sin\phi \tag{30}$$

3. Proper generalized decomposition for the resolution of the Reynolds equation

3.1. Separated representation related to the Reynolds equation

To analyze the lubricating film, the Reynolds equation Eq. (6) is formulated by PGD to find different parameters, like pressure distribution.

Consider the solution to the Reynolds equation (Eq. (6)) in a two-dimensional rectangular domain $\Omega = \Omega_\theta \times \Omega_z = (0, 2\pi) \times (-L/2, L/2)$. For all suitable test functions P^*, we consider the global weak form of Eq. (6):

$$\int_{\Omega\theta\times\Omega z} P^*\left[\frac{3}{hR_a^2}\frac{\mathrm{d}h}{\mathrm{d}\theta}\frac{\partial P}{\partial\theta} + \frac{1}{R_a^2}\frac{\partial^2 P}{\partial\theta^2} + \frac{\partial^2 P}{\partial z^2} - 6\frac{\mu\omega\mathrm{d}h}{h^3\mathrm{d}\theta}\right]\mathrm{d}\theta\mathrm{d}z = 0 \tag{31}$$

Our goal is to obtain a PGD approximate solution to Eq. (6) in the separated form

$$P(\theta, z) = \sum_{i=1}^{N} X_i(\theta)\cdot Y_i(z) \tag{32}$$

we shall do so by computing each term of the expansion one at a time, thus enriching the PGD approximation until a suitable convergence criterion is satisfied.

3.2. Progressive construction of the separated representation

At each enrichment step n ($n \geq 1$), we have already computed the $n-1$ first terms of the PGD approximation Eq. (32):

$$P^{n-1}(\theta, z) = \sum_{i=1}^{n-1} X_i(\theta)\cdot Y_i(z) \tag{33}$$

We now wish to compute the next term $X_n(\theta)\cdot V, Y_n(z)$ to obtain the enriched PGD solution

$$P^n(\theta,z) = P^{n-1}(\theta,z) + X_n(\theta)\cdot Y_n(z) = \sum_{i=1}^{n-1} X_i(\theta)\cdot Y_i(z) + X_n(\theta)\cdot Y_n(z), \tag{34}$$

both functions $X_n(\theta)\cdot Y_n(z)$ are unknown at the current enrichment step n, and they appear in the form of a product. The resulting problem is thus non-linear, and a suitable iterative scheme is required. We shall use the index q to denote a particular iteration.

At enrichment step n, the PGD approximation $P^{n,q}$ obtained at iteration q thus reads

$$P^{n,q}(\theta,z) = P^{n-1}(\theta,z) + X_n^q(\theta)\cdot Y_n^q(z) \tag{35}$$

The simplest iterative scheme is an alternating direction strategy that computes $X_n^q(\theta)$ from $Y_n^{q-1}(z)$, and then $Y_n^q(z)$ from $X_n^q(\theta)$. An arbitrary initial guess $Y_n^0(z)$ is specified to start the iterative process. The non-linear iterations proceed until reaching a fixed point within a user-specified tolerance ξ, i.e.

$$\frac{\left\| X_n^q(\theta)\cdot Y_n^q(z) - X_n^{q-1}(\theta)\cdot Y_n^{q-1}(z) \right\|_{L^2(\Omega)}}{\left\| X_n^{q-1}(\theta)\cdot Y_n^{q-1}(z) \right\|_{L^2(\Omega)}} < \xi \tag{36}$$

The enrichment step n thus ends with the assignments $X_n(\theta) \leftarrow X_n^q(\theta)$ and $Y_n(z) \leftarrow Y_n^q(z)$.The enrichment process itself stops when an appropriate measure of error $\kappa(n)$ becomes small enough, i.e. $\kappa(n) < \tilde{\xi}$ (a chosen enrichment tolerance). The corresponding stopping criterion is based on the norm (L^2) of mode n with respect to the norm of the first mode, i.e.

$$\kappa(n) = \frac{\|X_n(\theta)\cdot Y_n(z)\|_{L^2(\Omega)}}{\|X_1(\theta)\cdot Y_1(z)\|_{L^2(\Omega)}} \tag{37}$$

We now describe in more detail one particular alternating direction iteration at a given enrichment step.

3.2.1. Alternating direction strategy

Each iteration of the alternating direction scheme consists in the following two steps:

1. Computing $X_n^q(\theta)$ from $Y_n^{q-1}(z)$:
   In this case, the approximation reads

$$P^{n,q}(\theta,z) = \sum_{i=1}^{n-1} X_i(\theta)\cdot Y_i(z) + X_n^q(\theta)\cdot Y_n^{q-1}(z) \tag{38}$$

   where all functions are known except $X_n^q(\theta)$. The simplest choice for the weight function P^* in the weighted residual formulation (Eq. (31)) is

$$P^*(\theta,z) = X_n^*(\theta)\cdot Y_n^{q-1}(z) \tag{39}$$

   Injecting Eq. (38) and Eq. (39) into Eq. (31), we obtain

$$\begin{aligned}
&\int_{\Omega\theta\times\Omega z} X_n^*(\theta)\cdot Y_n^{q-1}(z)\cdot G_1\cdot \frac{\mathrm{d}X_n^q(\theta)}{\mathrm{d}\theta}\cdot Y_n^{q-1}(z)\cdot \mathrm{d}\theta\,\mathrm{d}z \\
&+ \frac{1}{R_a^2}\int_{\Omega\theta\times\Omega z} X_n^*(\theta)\cdot Y_n^{q-1}(z)\cdot \frac{\mathrm{d}^2X_n^q(\theta)}{\mathrm{d}\theta^2}\cdot Y_n^{q-1}(z)\cdot \mathrm{d}\theta\,\mathrm{d}z \\
&+ \int_{\Omega\theta\times\Omega z} X_n^*(\theta)\cdot Y_n^{q-1}(z)\cdot X_n^q(\theta)\cdot \frac{\mathrm{d}^2Y_n^{q-1}(z)}{\mathrm{d}\theta^2}\cdot \mathrm{d}\theta\,\mathrm{d}z \\
&+ \int_{\Omega\theta\times\Omega z} X_n^*(\theta)\cdot Y_n^{q-1}(z)\cdot G_1\cdot \sum_{i=1}^{n}\frac{\mathrm{d}X_i(\theta)}{\mathrm{d}\theta}\cdot Y_i(z)\cdot \mathrm{d}\theta\,\mathrm{d}z \\
&+ \frac{1}{R_a^2}\int_{\Omega\theta\times\Omega z} X_n^*(\theta)\cdot Y_n^{q-1}(z)\cdot \sum_{i=1}^{n}\frac{\mathrm{d}^2X_i(\theta)}{\mathrm{d}\theta^2}\cdot Y_i(z)\cdot \mathrm{d}\theta\,\mathrm{d}z
\end{aligned} \tag{40}$$

$$+\int_{\Omega\theta\times\Omega z} X_n^*(\theta)\cdot Y_n^{q-1}(z)\cdot\sum_{i=1}^{n} X_i(\theta)\cdot\frac{\mathrm{d}^2 Y_i(z)}{\mathrm{d}z^2}\cdot\mathrm{d}\theta\mathrm{d}z$$
$$-\int_{\Omega\theta\times\Omega z} X_n^*(\theta)\cdot Y_n^{q-1}(z)\cdot G_2\cdot\mathrm{d}\theta\mathrm{d}z=0$$

with $G_1=\frac{3}{hR_a^2}\frac{\mathrm{d}h}{\mathrm{d}\theta}$ and $G_2=\frac{6\mu w\mathrm{d}h}{h^3\cdot\mathrm{d}\theta}$.
Here comes a crucial point: since all functions of z are known in the above expression, we can compute the following one-dimensional integrals over Ωz:

$$\begin{cases}\alpha^\theta=\int_{\Omega z}\left(Y_n^{q-1}(z)\right)^2\mathrm{d}z\\ \beta^\theta=\int_{\Omega z}Y_n^{q-1}(z)\cdot\frac{\mathrm{d}^2Y_i(z)}{\mathrm{d}z^2}\mathrm{d}z\\ \gamma_i^\theta=\int_{\Omega z}Y_n^{q-1}(z)\cdot Y_i(z)\mathrm{d}z\\ \delta_i^\theta=\int_{\Omega z}Y_n^{q-1}(z)\cdot\frac{\mathrm{d}^2Y_i(z)}{\mathrm{d}z^2}\mathrm{d}z\\ \zeta^\theta=\int_{\Omega z}Y_n^{q-1}(z)\cdot G_2\mathrm{d}z\end{cases}\tag{41}$$

Equation (40) reduces to:

$$\begin{aligned}&\int_{\Omega\theta}X_n^*\cdot\alpha^\theta\cdot G_1\frac{\mathrm{d}X_n^q(\theta)}{\mathrm{d}\theta}\cdot\mathrm{d}\theta+\frac{1}{R_a^2}\int_{\Omega\theta}X_n^*\cdot\alpha^\theta\cdot\frac{\mathrm{d}^2X_n^q(\theta)}{\mathrm{d}\theta^2}\cdot\mathrm{d}\theta+\sum_{i=1}^{n-1}X_i(\theta)\frac{\mathrm{d}^2Y_i(z)}{\mathrm{d}z^2}\cdot\mathrm{d}\theta+\int_{\Omega\theta}X_n^*\cdot\beta^\theta\cdot X_n^q\cdot\mathrm{d}\theta\\ &=-\int_{\Omega\theta}X_n^*\cdot G_1\cdot\sum_{i=1}^{n-1}(\gamma_i^\theta\frac{\mathrm{d}X_i(\theta)}{\mathrm{d}\theta})\cdot\mathrm{d}\theta-\frac{1}{R_a^2}\int_{\Omega\theta}X_n^*\cdot\sum_{i=1}^{n-1}(\gamma_i^\theta\frac{\mathrm{d}^2X_i(\theta)}{\mathrm{d}\theta^2})\cdot\mathrm{d}\theta\\ &\quad-\int_{\Omega\theta}X_n^*\cdot\sum_{i=1}^{n-1}(\delta_i^\theta X_i(\theta))\cdot\mathrm{d}\theta+\int_{\Omega\theta}X_n^*\cdot\zeta^\theta\cdot\mathrm{d}\theta\end{aligned}\tag{42}$$

We have thus obtained the weighted residual form of a one-dimensional problem defined over $\Omega\theta$ that can be solved by using any discretization technique operating on the model weak form (finite element method, finite volumes) to obtain the function X_n^q we are looking for. Another possibility consists in coming back to the strong form of Eq. (42):

$$\begin{aligned}&\alpha^\theta\cdot G_1\cdot\frac{\mathrm{d}X_n^q(\theta)}{\mathrm{d}\theta}+\frac{1}{R_a^2}\cdot\alpha^\theta\cdot\frac{\mathrm{d}^2X_n^q(\theta)}{\mathrm{d}\theta^2}+\beta^\theta\cdot X_n^q\\ &=-G_1\cdot\sum_{i=1}^{n-1}\gamma_i^\theta\cdot\frac{\mathrm{d}X_i(\theta)}{\mathrm{d}\theta}-\frac{1}{R_a^2}\cdot\sum_{i=1}^{n-1}\gamma_i^\theta\cdot\frac{\mathrm{d}^2X_i(\theta)}{\mathrm{d}\theta^2}-\sum_{i=1}^{n-1}\delta_i^\theta\cdot X_i(\theta)+\zeta^\theta\end{aligned}\tag{43}$$

This could be solve it numerically by means of any suitable numerical method (Finite Differences, Pseudo-Spectral Techniques, etc.). The strong form Eq. (43) is a second-order ordinary differential equation for X_n^q.
Having thus computed $X_n^q(\theta)$, we are now ready to proceed with the second step of iteration q.

2. Computing $Y_n^q(z)$ from $X_n^q(\theta)$:
The procedure exactly mirrors what we have done above. Indeed, we simply exchange the roles played by all relevant functions of θ and z.
The current PGD approximation reads

$$P^{n,q}(\theta,z)=\sum_{i=1}^{n-1}X_i(\theta)\cdot Y_i(z)+X_n^q(\theta)\cdot Y_n^q(z)\tag{44}$$

where all functions are known except $Y_n^q(z)$.
The Galerkin formulation of Eq. (31) is obtained with the particular choice

$$P^*(\theta,z)=X_n^q(\theta)\cdot Y_n^*(z)\tag{45}$$

Then, by introducing (44) and (45) into (31), we get

$$\begin{aligned}
&\int_{\Omega\theta\times\Omega z} X_n^q(\theta)\cdot Y_n^*(z)\cdot G_1\cdot\frac{\mathrm{d}X_n^q(\theta)}{\mathrm{d}\theta}\cdot Y_n^q(z)\cdot\mathrm{d}\theta\mathrm{d}z+\frac{1}{R_a^2}\int_{\Omega\theta\times\Omega z} X_n^q(\theta)\cdot Y_n^*(z)\cdot\frac{\mathrm{d}^2X_n^q(\theta)}{\mathrm{d}\theta^2}\cdot Y_n^q(z)\cdot\mathrm{d}\theta\mathrm{d}z\\
&+\int_{\Omega\theta\times\Omega z} X_n^q(\theta)\cdot Y_n^*(z)\cdot\frac{\mathrm{d}^2Y_n^q(z)}{\mathrm{d}z^2}\cdot X_n^q(\theta)\cdot\mathrm{d}\theta\mathrm{d}z=-\int_{\Omega\theta\times\Omega z} X_n^q(\theta)\cdot Y_n^*(z)\cdot G_1\cdot\sum_{i=1}^{n-1}\frac{\mathrm{d}X_i(\theta)}{\mathrm{d}\theta}\cdot Y_i(z)\mathrm{d}\theta\mathrm{d}z\\
&-\frac{1}{R_a^2}\int_{\Omega\theta\times\Omega z} X_n^q(\theta)\cdot Y_n^*(z)\cdot\frac{\mathrm{d}^2X_i(\theta)}{\mathrm{d}\theta^2}\cdot Y_i(z)\cdot\mathrm{d}\theta\mathrm{d}z\\
&-\int_{\Omega\theta\times\Omega z} X_n^q(\theta)\cdot Y_n^*(z)\cdot\sum_{i=1}^{n-1}\frac{\mathrm{d}^2Y_i(z)}{\mathrm{d}z^2}\cdot X_i(\theta)\cdot\mathrm{d}\theta\mathrm{d}z+\int_{\Omega\theta\times\Omega z} X_n^q(\theta)\cdot Y_n^*(z)\cdot G_2\cdot\mathrm{d}\theta\mathrm{d}z
\end{aligned}\tag{46}$$

with $G_1=\frac{3}{hR_a^2}\frac{\mathrm{d}h}{\mathrm{d}\theta}$ and $G_2=\frac{6\mu w\mathrm{d}h}{h^3\mathrm{d}\theta}$.
As all functions of θ are known, the integrals over $\Omega\theta$ can be computed to obtain

$$\begin{cases}
\alpha^z=\int_{\Omega\theta}\left(X_n^q(\theta)\right)^2\mathrm{d}\theta\\
\psi^z=\int_{\Omega\theta}X_n^q(\theta)\frac{\mathrm{d}X_n^q(\theta)}{\mathrm{d}\theta}\mathrm{d}\theta\\
\beta^z=\int_{\Omega\theta}X_n^q(\theta)\cdot\frac{\mathrm{d}^2X_n^q(\theta)}{\mathrm{d}\theta^2}\mathrm{d}\theta\\
\gamma_i^z=\int_{\Omega\theta}X_n^q(\theta)\cdot X_i(\theta)\mathrm{d}\theta\\
\delta_i^z=\int_{\Omega\theta}X_n^q(\theta)\cdot\frac{\mathrm{d}^2X_i(\theta)}{\mathrm{d}\theta^2}\mathrm{d}\theta\\
\phi_i^z=\int_{\Omega\theta}X_n^q(\theta)\cdot\frac{\mathrm{d}X_i(\theta)}{\mathrm{d}\theta}\mathrm{d}\theta\\
\zeta^z=\int_{\Omega\theta}X_n^q(\theta)\cdot G_2\mathrm{d}\theta
\end{cases}\tag{47}$$

Equation (46) becomes

$$\begin{aligned}
&\int_{\Omega z}\psi^z\cdot Y_n^*(z)\cdot G_1\cdot Y_n^q(z)\mathrm{d}z+\frac{1}{R_a^2}\int_{\Omega z}\beta^z\cdot Y_n^*(z)\cdot Y_n^q(z)\cdot\mathrm{d}z+\int_{\Omega z}\alpha^z\cdot Y_n^*(z)\cdot\frac{\mathrm{d}^2Y_n^q(z)}{\mathrm{d}z^2}\cdot\mathrm{d}z\\
&=-\int_{\Omega z}Y_n^*(z)\cdot G_1\cdot\sum_{i=1}^{n-1}\phi_i^z\cdot Y_i(z)\cdot\mathrm{d}z-\frac{1}{R_a^2}\int_{\Omega z}Y_n^*(z)\cdot\sum_{i=1}^{n-1}\delta_i^z\cdot Y_i(z)\cdot\mathrm{d}z\\
&-\int_{\Omega z}Y_n^*(z)\cdot\sum_{i=1}^{n-1}\gamma_i^z\frac{\mathrm{d}^2Y_i(z)}{\mathrm{d}z^2}\cdot\mathrm{d}z+\int_{\Omega z}Y_n^*(z)\cdot\zeta^z\cdot\mathrm{d}z
\end{aligned}\tag{48}$$

As before, we have thus obtained the weighted residual form of an elliptic problem defined over Ωz whose solution is the function $Y_n^q(z)$. Alternatively, the corresponding strong formulation of this one-dimensional problem reads

$$\begin{aligned}
&\psi^z\cdot G_1\cdot Y_n^q(z)+\frac{1}{R_a^2}\cdot\beta^z\cdot Y_n^q(z)+\alpha^z\frac{\mathrm{d}^2Y_n^q(z)}{\mathrm{d}z^2}=-G_1\cdot\sum_{i=1}^{n-1}\phi_i^z\cdot Y_i(z)-\frac{1}{R_a^2}\cdot\sum_{i=1}^{n-1}\delta_i^z\cdot Y_i(z)-\sum_{i=1}^{n-1}\gamma_i^z\cdot\frac{\mathrm{d}^2Y_i(z)}{\mathrm{d}z^2}\\
&+\zeta^z
\end{aligned}\tag{49}$$

3.3. PGD program description

The algorithm of the PGD source code implemented in Matlab is given in Algorithm 1. The procedure is as follows.

1. The bearing characteristics are defined.
2. When the geometry of the problem domain is created, a set of field nodes is generated to represent the problem domain.
3. A progressive construction of the separated representation is performed through two loops; the outer loop is for the main enrichment procedure, stopping when the criterion (Eq. (37)) is satisfied, and the boundary conditions are applied. In the inner loop, the non-linear iterations proceed until reaching a fixed point within the tolerance defined in Eq. (36); the detailed procedure is described in Algorithm 1.

4. The separated representation is reconstructed to obtain pressure solution.
5. Post-processing is performed to obtain results in terms of load carrying capacity, Sommerfeld and friction numbers.

Algorithm 1 Pseudo-code of the implemented PGD approach.

```
Input data (bearing characteristics, geometry mesh, ξ, ξ̃, maximum number of enrichments (Max_terms), maximum number of iterations in the fixed point loop (Max_fp))
Mesh definition for each dimension: N_θ, N_z
for i = 1:Max_terms do (main enrichment loop)
    Initialization of the fixed point loop: S_θ = random(N_θ, 1), S_z = random(N_z, 1)
    Definition of the boundary conditions
    for j = 1:Max_fp do (fixed point iterations)
        Store the old values of S_θ and S_z for later comparison
        procedure Alternating Direction Strategy
            Solve for S_θ the system of one-dimensional integrals (Eq. (41))
            Construction of the finite difference solution for the strong form given in Eq. (43)
            Solve for S_z the system of one-dimensional integrals (Eq. (47))
            Construction of the finite-difference solution for the strong form given in Eq. (49)
        Norm of the difference S_diff between the two fixed point iterations (Eq. (36))
        if S_diff < ξ then
            Break (stopping from fixed point iterations)
    Computation of the error κ (Eq. (37))
    if κ < ξ̃ then (verification of the second stopping criterion)
        Break (stopping from the main enrichment loop)
```

4. Numerical results and discussions

In this section, the accuracy and the efficiency of PGD method are investigated through several benchmark examples. In the first part, a comparison of the evaluated fluid film pressure distribution obtained from PGD, FDM, FDM_{sor} and analytical solution in the cases of infinitely short and long journal bearing (ISJB, ILJB) is presented. This comparison is extended to the evaluation of the journal bearing characteristics (load carrying capacity, Sommerfeld and friction numbers). A final comparison is carried out in terms of CPU time consuming for all the above-mentioned numerical methods. In the second part, the same comparisons are performed for the finite journal bearing (FJB) with different L/D ratios.
We note that, for the following study, the PGD associated parameters are chosen as follows:

- termination criterion for the fixed point iterations: $\xi = 10^{-8}$,
- termination criterion used for the enrichment process: $\tilde{\xi} = 10^{-5}$,
- maximum number of enrichments: $Max_{\text{terms}} = 4$,
- maximum number of iterations in the fixed point loop: $Max_{\text{fp}} = 20$.

In the case of finite difference formulation, central difference scheme of spacial discretization is used to numerically solve the Reynolds equation. Successive Over Relaxation (SOR) ($\Omega_{\text{SOR}} = 2$) of the Finite Difference Method is also employed in order to accelerate the convergence process.

4.1. Error index

In order to check the accuracy of the obtained solutions, the definition of a specific error index is necessary. The relative error on the pressure computation is defined as follows:

$$E_P = \frac{\left\| \widehat{P} - P \right\|_{L^2(\Omega)}}{\| P \|_{L^2(\Omega)}} \tag{50}$$

where $\widehat{P}$ and P are the pressures computed by the used numerical methods and the exact analytical solution, respectively. In order to evaluate the convergence rates of each numerical methods, we introduce a characteristic length h_{mesh}. For a grid of rectangular cells:

$$h_{\text{mesh}} = \sqrt{\frac{A_\Omega}{n_c}} \tag{51}$$

where A_Ω is the area of the problem domain and n_c the number of cells.

4.2. Infinitely short and long journal bearing

4.2.1. Pressure distribution

In the present section, the following input data associated with the problem of journal bearing lubrication are used (Table 1).

The pressure distribution fields obtained numerically by PGD (with a regular mesh $= 100 \times 100$ nodes) for the infinitely short journal bearing ($L/D = 0.12$) and infinitely long journal bearing ($L/D = 6$) are illustrated in Figs. 2 and 3, respectively.

Table 1
Journal bearing and lubricant characteristics.

	Parameters	Infinitely short journal bearing	Infinitely long journal bearing
L	journal length	$6{\cdot}10^{-3}$ m	$300{\cdot}10^{-3}$ m
D	journal diameter	$50{\cdot}10^{-3}$ m	$50{\cdot}10^{-3}$ m
C	radial clearance	$20{\cdot}10^{-6}$ m	$20{\cdot}10^{-6}$ m
ϵ	eccentricity ratio	0.1	0.1
N	journal rotation speed	1000 rpm	1000 rpm
μ	lubricant dynamic viscosity	0.19 Pa·s	0.19 Pa·s
	mesh	100×100 nodes	100×100 nodes

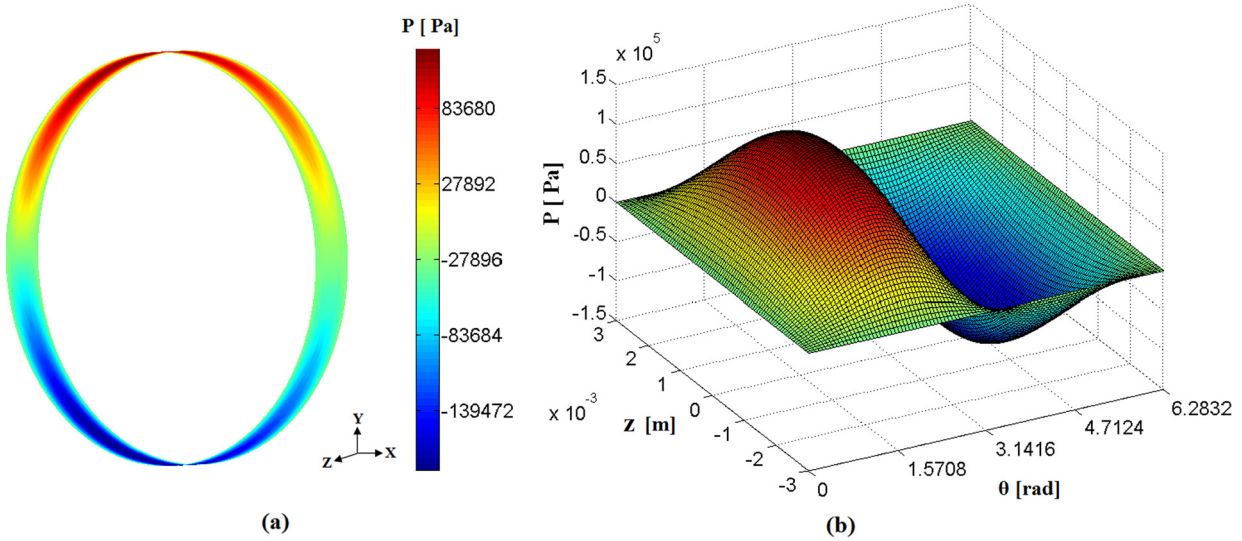

Fig. 2. Pressure distribution for ISJB ($L/D = 0.12$).

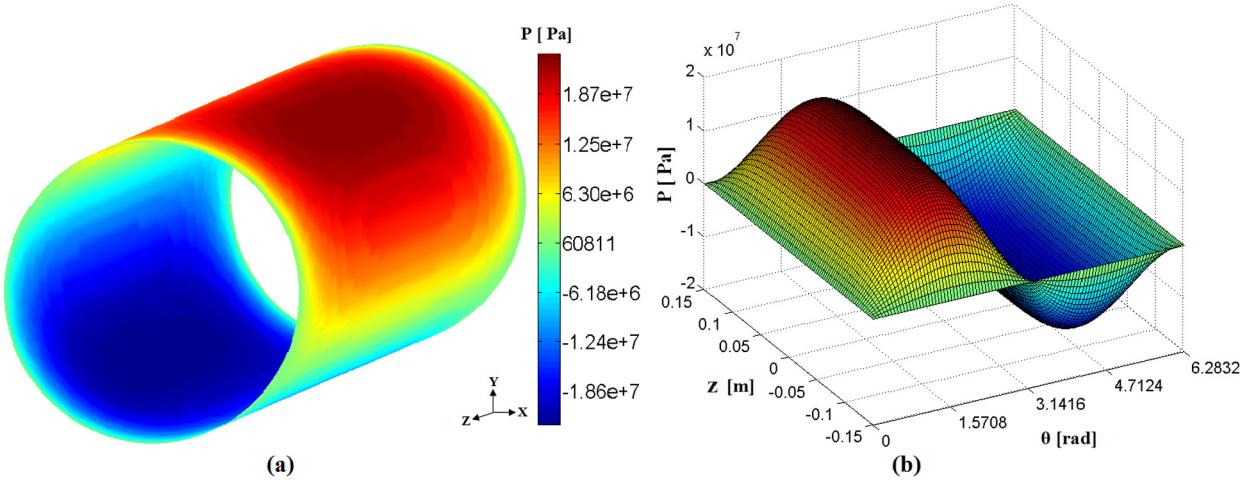

Fig. 3. Pressure distribution for ILJB ($L/D = 6$).

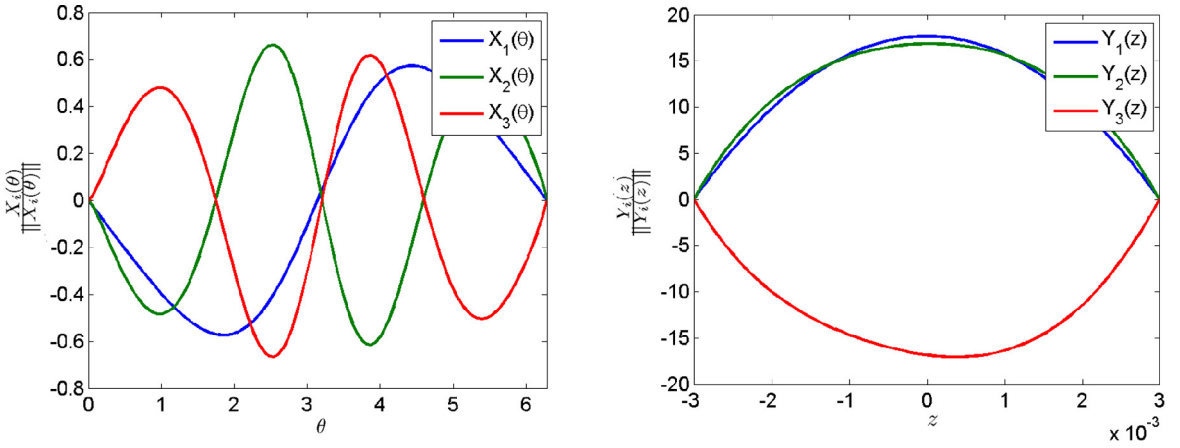

Fig. 4. Normalized functions for ISJB: $X_i(\theta)$ (left) and $Y_i(z)$ (right) with $i = 1, ..., 3$.

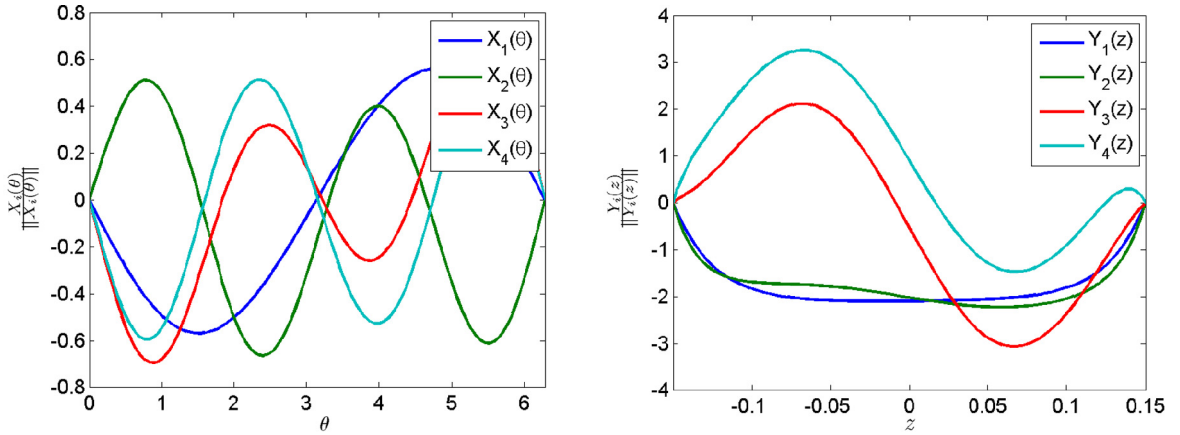

Fig. 5. Normalized functions for ILJB: $X_i(\theta)$ (left) and $Y_i(z)$ (right) with $i = 1, ..., 4$.

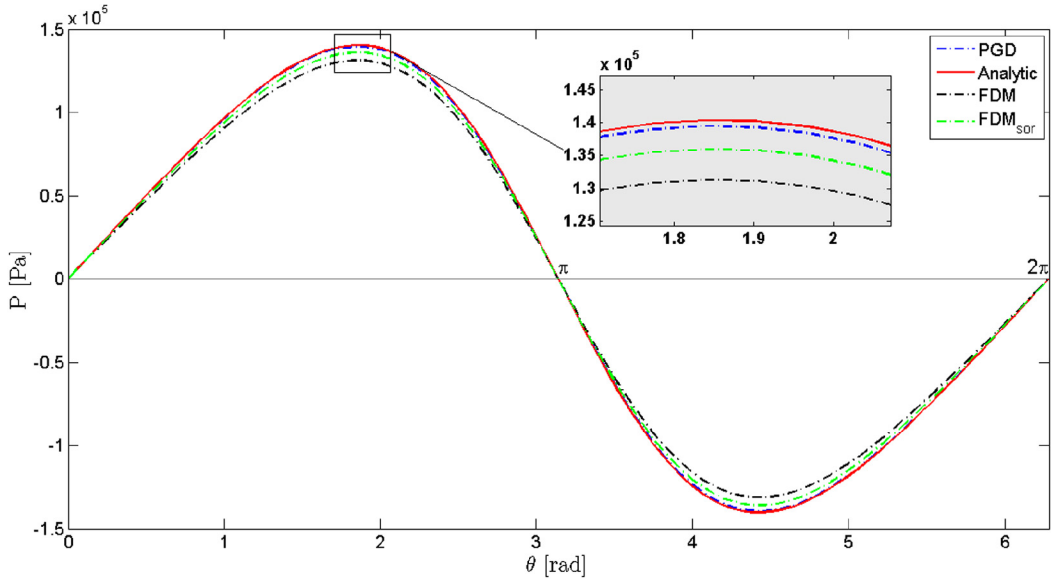

Fig. 6. Comparison of pressure distribution obtained by PGD, FDM, FDM_{sor}, and analytical solution at $z = 0$ for ISJB.

In Figs. 4 and 5, the normalized separated functions $X_i(\theta)$ and $Y_i(z)$ are illustrated for $i = 1, ..., 3$ and $i = 1, ..., 4$ respectively. It is noticed that for the computation of the PGD solution in the case of the ISJB problem, only three enrichment steps are needed (where the stopping criterion is satisfied), while in the case of the ILJB problem, all steps are carried out.

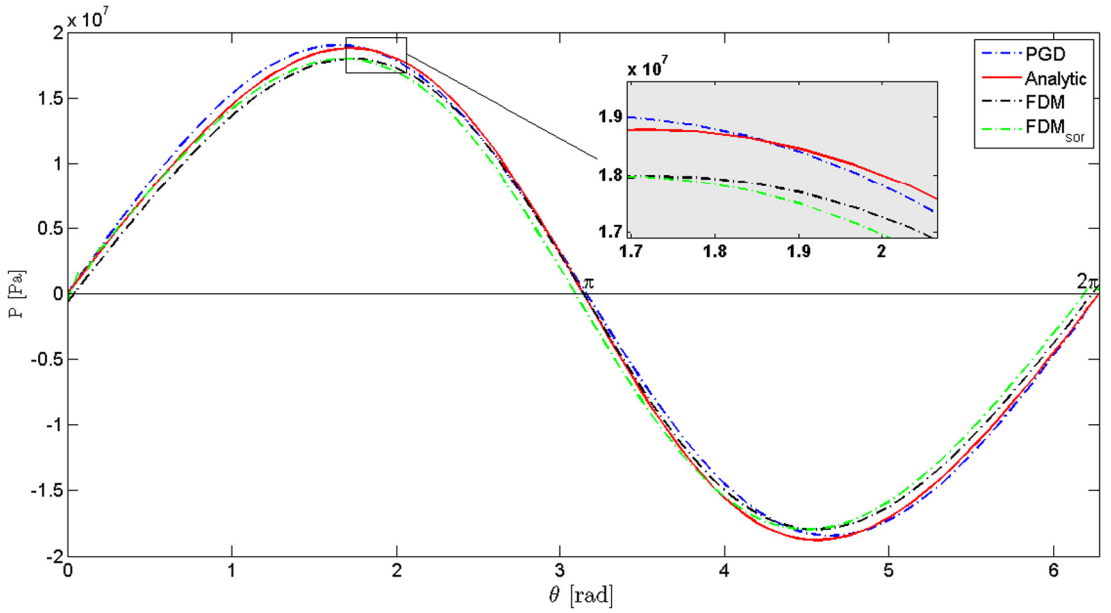

Fig. 7. Comparison of pressure distribution obtained by PGD, FDM, FDM_{sor}, and analytical solution at $z = 0$ for ILJB.

In Figs. 6 and 7, the pressure distribution obtained by PGD is plotted along the mid-line of the plain journal bearing ($z = 0$) and compared with the numerical solutions to FDM, FDM_{sor} and the analytical solutions. It is noticed that the pressure curves are quite close for all the approaches. However, the error level of the PGD method is smaller than those obtained by FDM and FDM_{sor}. For a more accurate comparison, a mesh convergence study is conducted in section 4.2.4 with the computation of the error norm (equation (50)).

We note that these first comparison tests of pressure distribution (given in Figs. 6 and 7) are calculated at half length ($z = 0$). These comparison tests are still insufficient to evaluate the pressure computation error in the whole domain. For a more correct comparison, the evaluation of the Sommerfeld and friction numbers, which requires the calculation of the integral of the pressure distribution over the whole domain (load carrying capacity), is performed in the next sections.

4.2.2. Sommerfeld number

In Table 2, the Sommerfeld number is calculated for ISJB and ILJB with increasing the eccentricity ratio ($\epsilon = 0.1$–0.9), using PGD, FDM and FDM_{sor} methods and compared with the results given in the reference [34].

Figs. 8 and 9 display the Sommerfeld number as a function of the eccentricity ratio in the cases of ISJB and ILJB. It is noticed that the Sommerfeld number calculated with the proposed method (PGD) agrees with the results obtained in [34] and other methods.

Table 2
Sommerfeld number for ISJB and ILJB with different values of eccentricity ratio.

Parameters		Eccentricity ratio ϵ								
L/D	Sommerfeld	0.1	0.2	0.3	0.4	0.5	0.6	0.7	0.8	0.9
SJB	$S(L/D)^2$-[34]	0.99	0.461	0.272	0.17	0.106	0.0625	0.033	0.0139	0.00331
	$S(L/D)^2$-PGD	0.99	0.464	0.273	0.17	0.106	0.0631	0.033	0.0140	0.00336
	$S(L/D)^2$-FDM	1.08	0.504	0.298	0.18	0.117	0.0694	0.037	0.0159	0.00506
	$S(L/D)^2$-FDM_{sor}	1.08	0.503	0.297	0.18	0.116	0.0694	0.037	0.0159	0.00405
LJB	S-[34]	0.247	0.123	0.0823	0.0628	0.0483	0.0389	0.0297	0.0211	0.0114
	S-PGD	0.395	0.192	0.123	0.0850	0.0601	0.0394	0.0194	0.0118	0.0050
	S-FDM	0.422	0.208	0.136	0.0980	0.0743	0.0566	0.0420	0.0286	0.0150
	S-FDM_{sor}	0.422	0.208	0.136	0.0980	0.0743	0.0566	0.0420	0.0286	0.0150

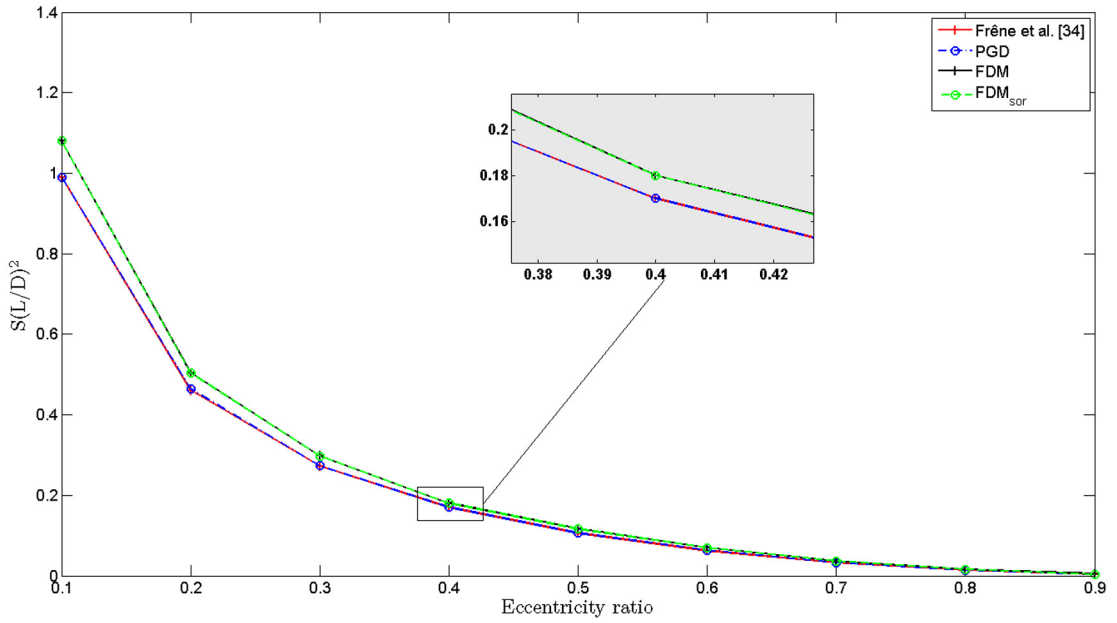

Fig. 8. Sommerfeld number with different values of the eccentricity ratio for ISJB.

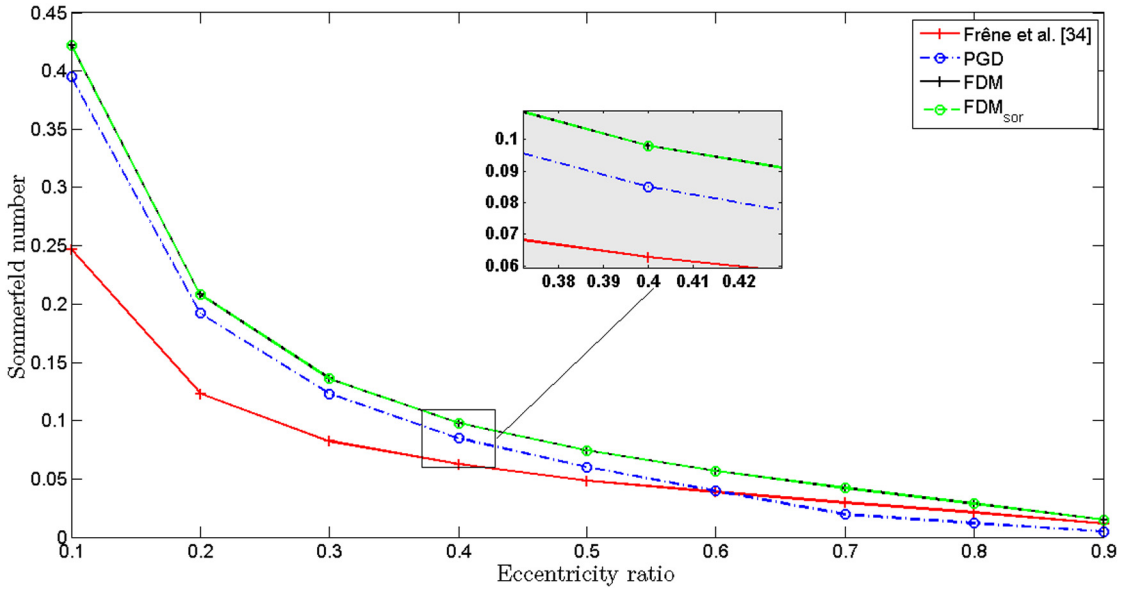

Fig. 9. Sommerfeld number with different values of the eccentricity ratio for ILJB.

4.2.3. Friction number

In Table 3, the friction number is calculated for ISJB and ILJB with increasing the eccentricity ratio ($\epsilon = 0.1$–0.9), using PGD, FDM, and FDM$_{sor}$ methods and compared with the results given in reference [34].

Figs. 10 and 11 show the friction number as a function of the eccentricity ratio in the cases of ISJB and ILJB. It is noticed that the friction number computed with the PGD method is in good correspondence with other results obtained in [34] and from FDM, FDM$_{sor}$ methods.

Table 3
Friction number for the ISJB and ILJB with different values of eccentricity ratio.

Parameters		Eccentricity ratio ϵ								
L/D	Friction number	0.1	0.2	0.3	0.4	0.5	0.6	0.7	0.8	0.9
ISJB	$f(L/D)^2$-[34]	18.75	8.514	4.98	3.14	2.016	1.25	0.722	0.355	0.114
	$f(L/D)^2$-PGD	19.75	9.348	5.66	3.69	2.437	1.55	0.921	0.463	0.152
	$f(L/D)^2$-FDM	21.43	10.145	6.15	4.01	2.649	1.69	1.005	0.507	0.169
	$f(L/D)^2$-FDM_{sor}	21.43	10.144	6.15	4.01	2.647	1.69	1.004	0.507	0.169
ILJB	f-[34]	5.02	2.61	1.84	1.47	1.25	1.10	0.98	0.852	0.658
	f-PGD	7.84	3.88	2.55	1.85	1.37	0.97	0.53	0.391	0.220
	f-FDM	8.3	4.02	2.55	1.76	1.25	0.85	0.51	0.189	0.150
	f-FDM_{sor}	8.36	4.16	2.76	2.04	1.60	1.29	1.04	0.817	0.560

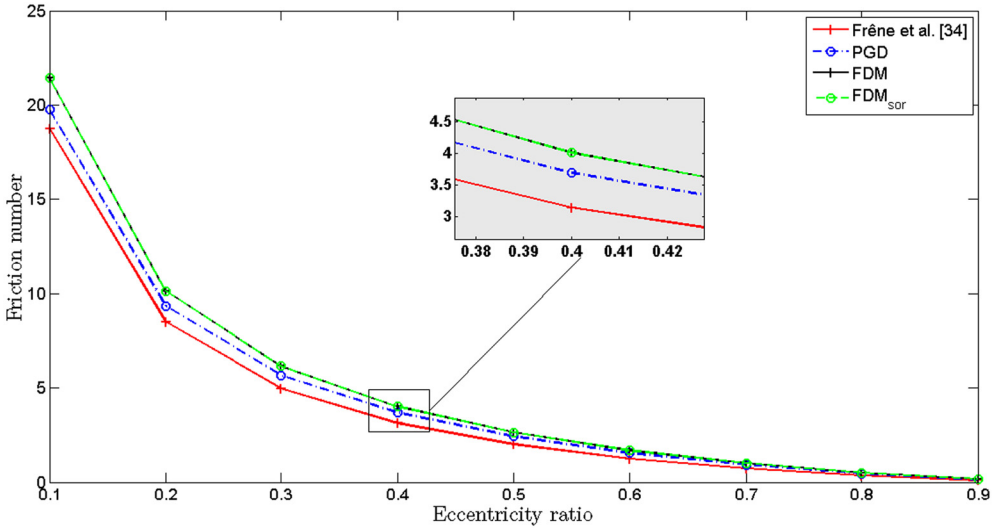

Fig. 10. Friction number with different values of the eccentricity ratio for ISJB.

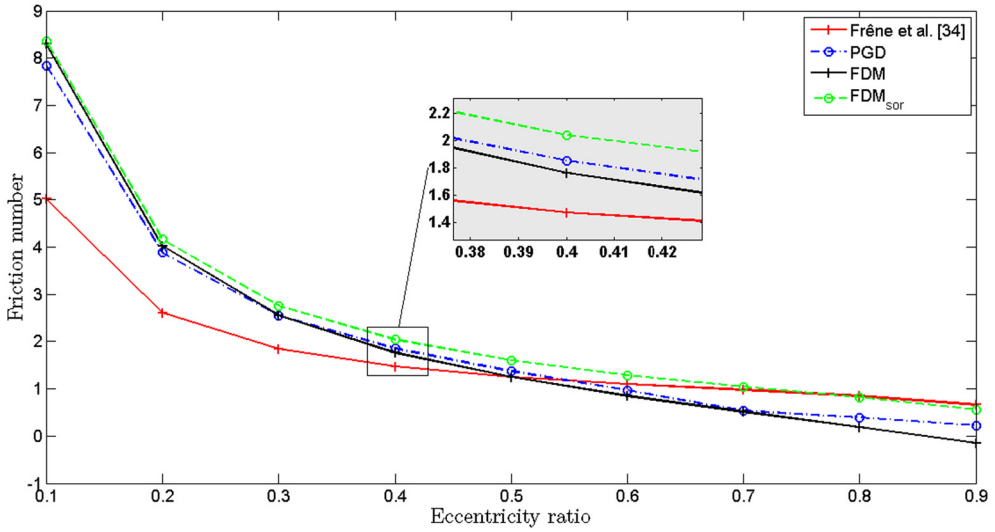

Fig. 11. Friction number with different values of the eccentricity ratio for ILJB.

4.2.4. Mesh convergence study

Different sets of regularly distributed nodes are employed: (20 × 20), (40 × 40), (70 × 70), (100 × 100), (200 × 200), (300 × 300), (400 × 400), (500 × 500), (600 × 600). The convergence curves of pressure field obtained from FDM, FDM_{sor} and PGD methods are listed in Table 4 and plotted in Figs. 12 and 13.

Table 4
Errors in pressure computation for ISJB and ILJB using FDM, FDM_{sor} and PGD methods.

Nodes	h_{mesh}	Error E_P for ISJB			h_{mesh}	Error E_P for ILJB		
		PGD	FDM	FDM_{sor}		PGD	FDM	FDM_{sor}
400	0.00970	0.006759	0.28120	0.10647	0.00686	0.11664	0.24676	0.36086
1600	0.00485	0.006759	0.14912	0.05986	0.00343	0.06696	0.12399	0.17724
4900	0.00277	0.006767	0.08931	0.03919	0.00196	0.04661	0.07264	0.10171
10000	0.00194	0.006767	0.06483	0.03114	0.00137	0.04291	0.05207	0.07206
40000	0.00097	0.006767	0.03589	0.02120	0.00068	0.03964	0.02833	0.03769
90000	0.00064	0.006767	0.02615	0.01767	0.00045	0.03901	0.02042	0.02629
160000	0.00048	0.006767	0.02127	0.01577	0.00038	0.03879	0.01648	0.02063
250000	0.00038	0.006767	0.01834	0.01454	0.00027	0.03869	0.01412	0.01726
360000	0.00032	0.006767	0.01639	0.01365	0.00022	0.03863	0.01254	0.01503

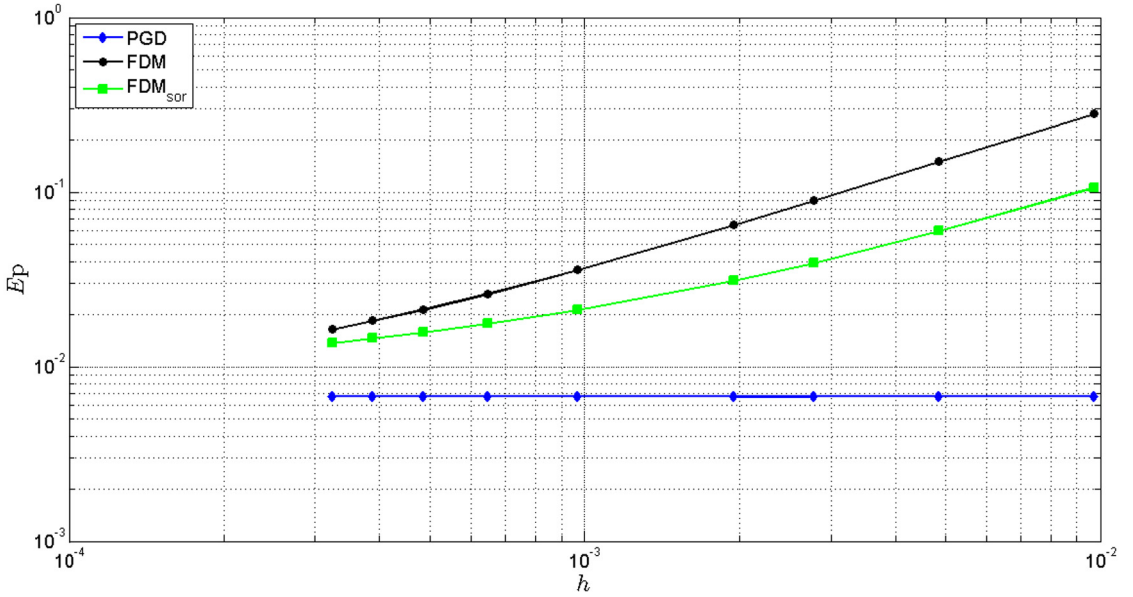

Fig. 12. Error in pressure computation for ISJB using FDM, FDM_{sor}, and PGD methods.

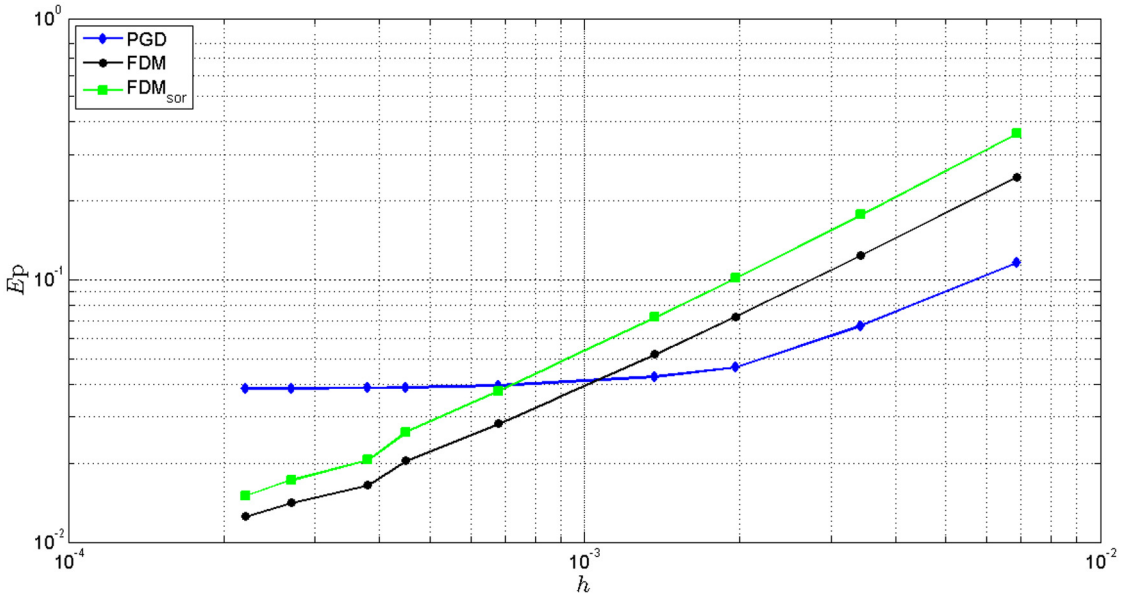

Fig. 13. Error in pressure computation for ILJB using FDM, FDM_{sor} and PGD methods.

Table 5
Comparison of computational time required for calculation of fluid film pressure using FEM, FEM_{sor}, and PGD.

Nodes	Computational time (s)					
	ISJB			ILJB		
	PGD	FDM	FDM_{SOR}	PGD	FDM	FDM_{SOR}
2500	0.08	0.14	0.16	0.10	0.15	0.17
10,000	0.09	0.79	0.86	0.11	0.81	0.87
40,000	0.15	21.06	21.49	0.19	21.11	21.28
90,000	0.33	123.08	125.25	0.42	122.67	124.59
160,000	0.64	401.97	406.99	0.69	395.07	397.65
250,000	0.95	981.70	992.09	1.07	979.91	988.56
360,000	1.22	2045.88	2057.86	1.55	2027.67	2272.35

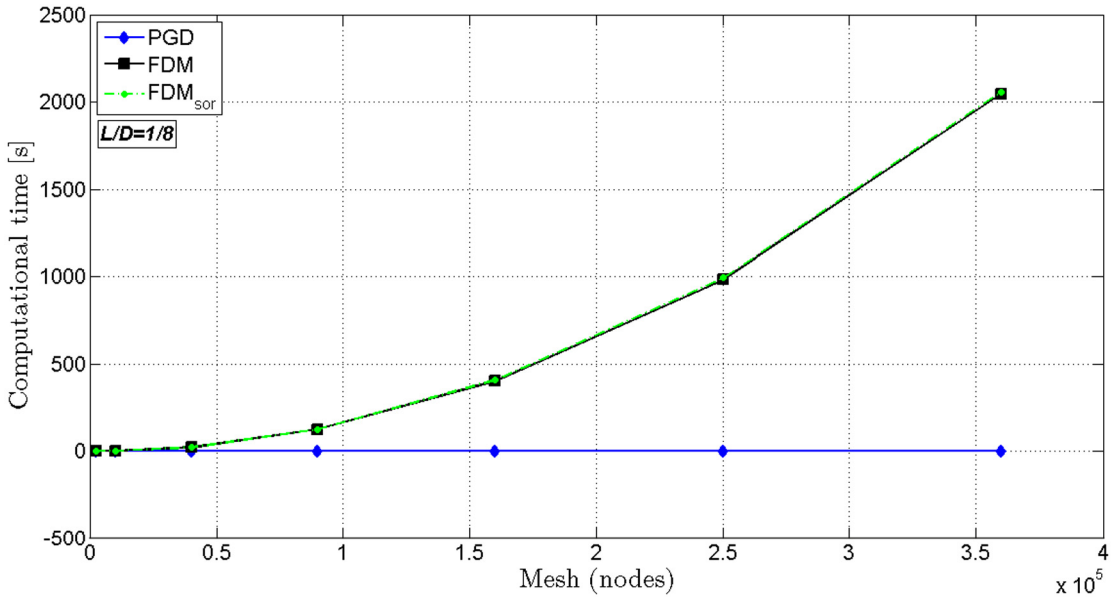

Fig. 14. FDM versus PGD computational time when increasing the number of nodes in ISJB ($L/D = 0.12$).

The convergence rate of the proposed approach (PGD) is relatively better than those obtained by FDM, FDM_{sor} methods. It is also noticed that the error in PGD computation have a tendency to stabilize immediately for the first mesh configurations. This is due to the enrichment iteration procedure of PGD, where the error stabilizes when the convergence rate is reached (i.e. until reaching the fixed point, Algorithm 1). In general, a finer mesh typically results in a more accurate solution. However, as a mesh is made finer, the computation time increases. Because of that, an investigation on the computational time required for the PGD resolution procedure is more than essential.

4.2.5. Computational time

The computational times required for the calculation of fluid film pressure with different mesh configurations using FDM, FDM_{sor} and PGD methods are listed in Table 5.

The computations are performed on Intel Core i5-2450M CPU @ 2.50 GHz (6 GB RAM, 64 bit) using Matlab. Figs. 14 and 15 illustrate the computational time when increasing the number of nodes using FDM, FDM_{sor} and PGD methods.

Through this comparison, the efficiency of PGD compared to other methods, in term of computational time, is quite clear. We notice that for an increasingly finer mesh, unlike other methods, PGD stay incredibly less time consuming. This is justified by the fact that in the PGD method, a separated representation of the spacial domain is performed, thus making the order of computations impressively reduced. More clarifications about the order of computations in PGD method are provided at the end of this paper.

4.3. Finite journal bearing

A more complete analysis of the capabilities of the proposed method can be done from the resolution of the Reynolds equation in the case of finite journal bearing (FJB) with different values of the L/D ratio.
Table 6 describes the model parameters related to the finite journal bearing considered in this case.

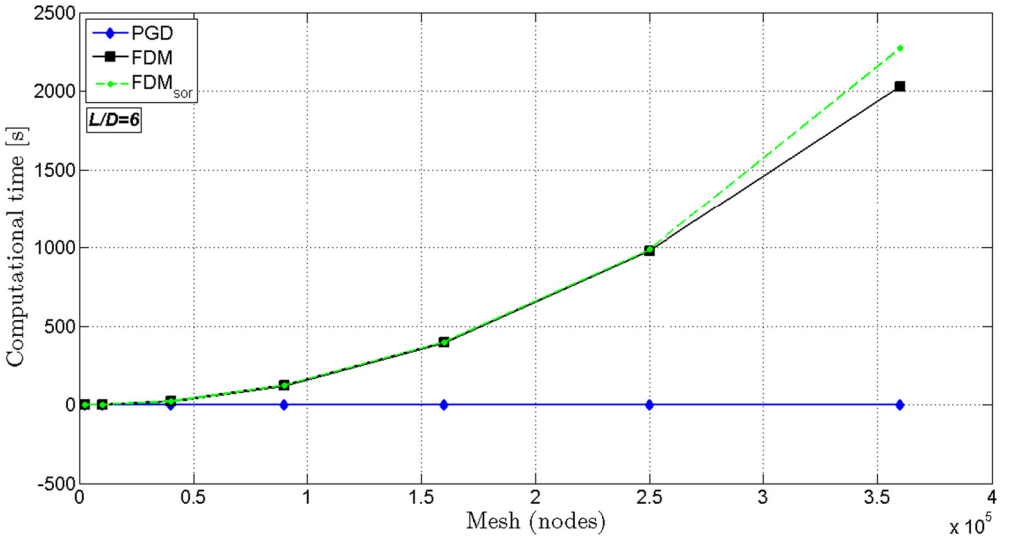

Fig. 15. FDM versus PGD computational time when increasing the number of nodes in ILJB ($L/D = 6$).

Table 6
Finite journal bearing characteristics and lubricant properties.

Parameters		Finite journal bearing			
L	journal length	0.0125 m	0.025 m	0.05 m	0.1 m
D	journal diameter	$50{\cdot}10^{-3}$ m			
L/D	ratio	1/4	1/2	1	2
C	radial clearance	$20{\cdot}10^{-6}$ m			
ϵ	eccentricity ratio	0.1∼0.9			
N	journal rotation speed	1000 rpm			
μ	lubricant dynamic viscosity	0.19 Pa·s			
	mesh	100×100 nodes			

4.3.1. Pressure distribution

The pressure distribution field obtained numerically by PGD (with a regular mesh $= 100 \times 100$ nodes) on the finite journal bearing with $L/D = 1$, as illustrated in Fig. 16.

In Fig. 17, the normalized separated functions $X_i(\theta)$ and $Y_i(z)$ are illustrated for $i = 1, \ldots, 4$. It is noticed that for the computation of the PGD solution in the case of FJB problem, all enrichment steps are carried out.

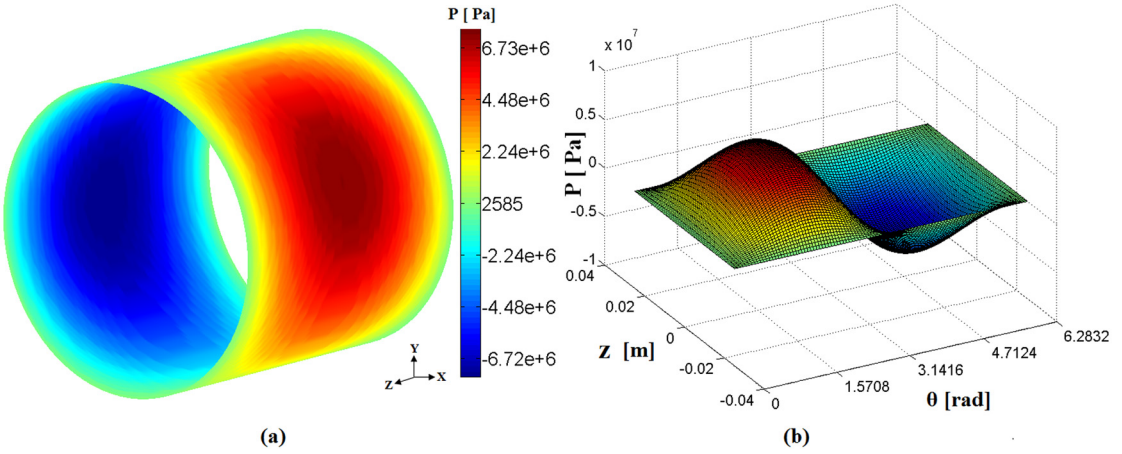

Fig. 16. Pressure distribution for FJB ($L/D = 1$) with $\varepsilon = 0.1$ (mesh size $= 100 \times 100$).

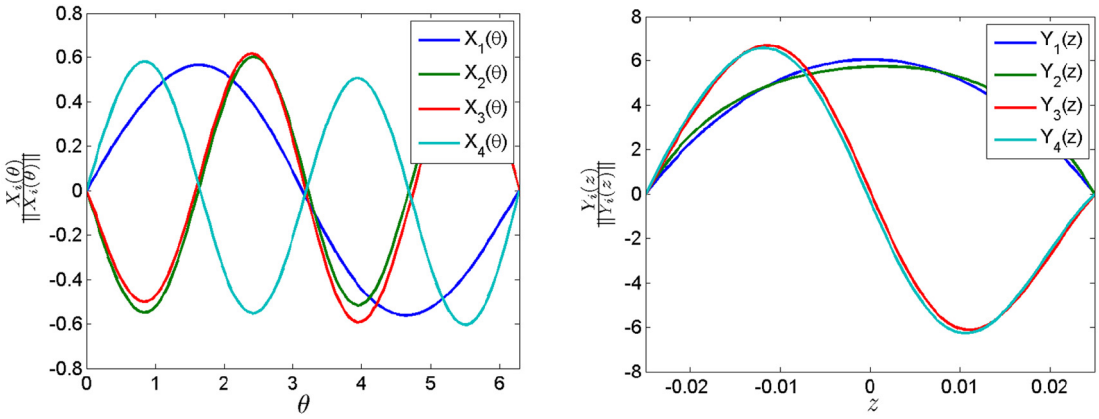

Fig. 17. Normalized function $X_i(\theta)$ (left) and $Y_i(z)$ (right) with $i = 1, ..., 4$.

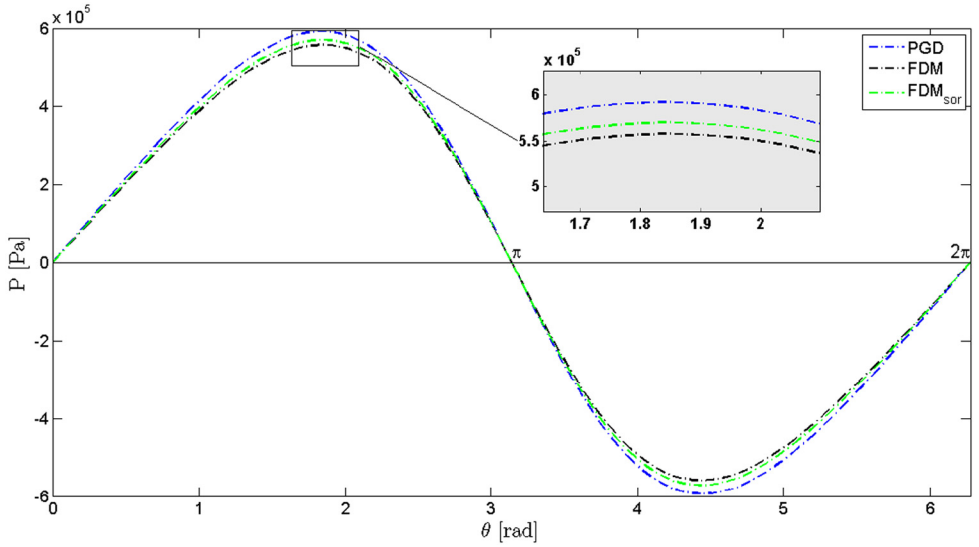

Fig. 18. Comparison of pressure distributions obtained by PGD, FDM, FDM_{sor} at $z = 0$ for FJB ($L/D = 1/4$).

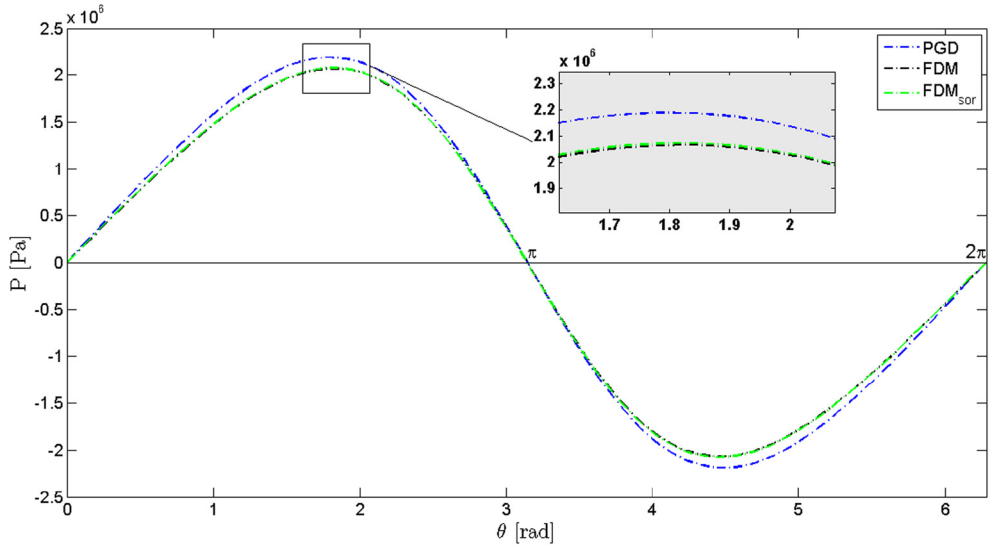

Fig. 19. Comparison of pressure distributions obtained by PGD, FDM, FDM_{sor} at $z = 0$ for FJB ($L/D = 1/2$).

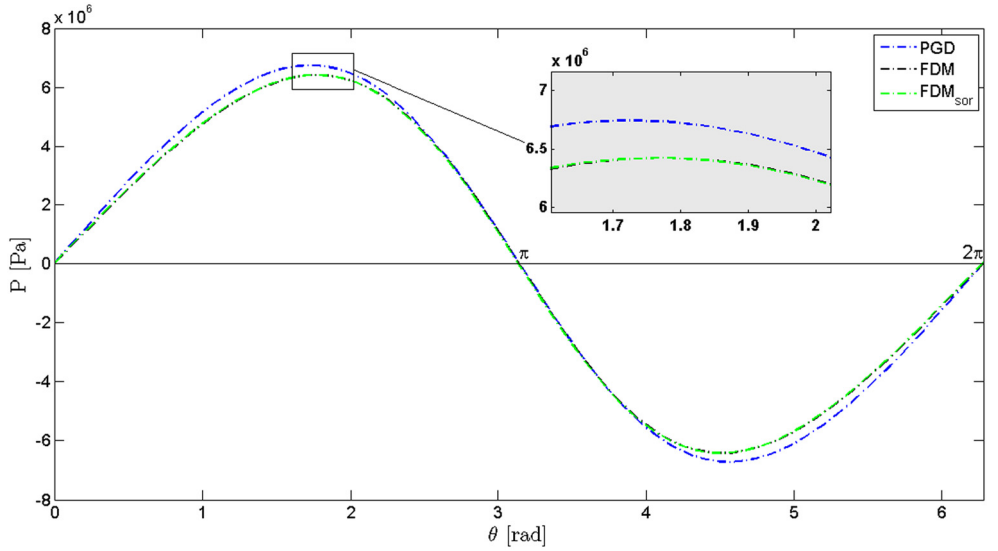

Fig. 20. Comparison of pressure distributions obtained by PGD, FDM, FDM_{sor} at $z = 0$ for FJB ($L/D = 1$).

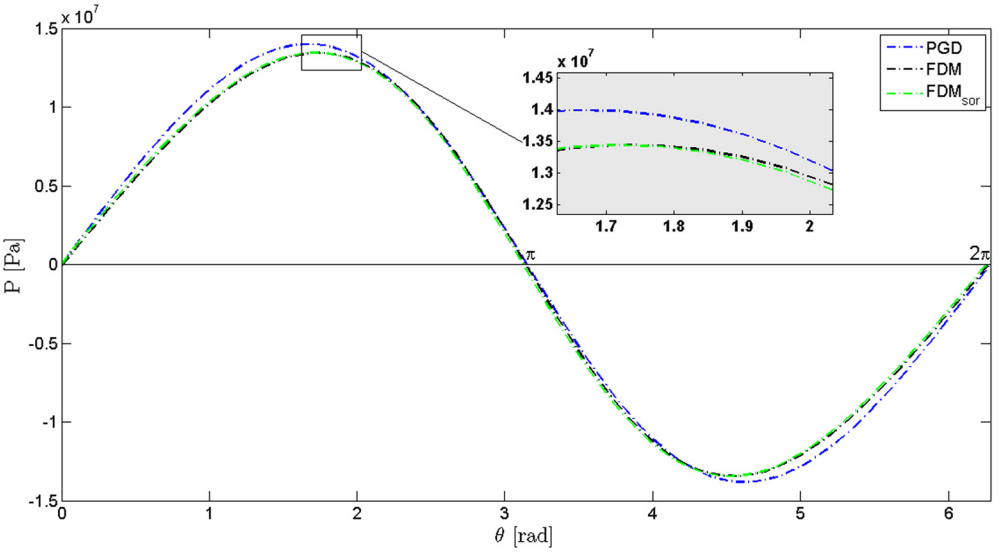

Fig. 21. Comparison of pressure distributions obtained by PGD, FDM, FDM_{sor} at $z = 0$ for FJB ($L/D = 2$).

In Figs. 18–21, the pressure distribution obtained by PGD along the mid-line of the plain journal bearing ($z = 0$) with different values of the L/D ratio ($L/D = 1/4, 1/2, 1, 2$) is plotted and compared with the numerical solutions to FDM, FDM_{sor}. It is noticed that the pressure curves are quite close for all the approaches. For more correct and global comparisons, the evaluation of the Sommerfeld and friction numbers is performed in the next sections.

4.3.2. Sommerfeld number

In Table 7, the Sommerfeld number is calculated for different L/D ratios with increasing the eccentricity ratio ($\epsilon = 0.1$–0.9), using PGD, FDM and FDM_{sor} methods, and compared with the results given in [34].

Figs. 22 to 25 display the Sommerfeld number as a function of the eccentricity ratio for different values of the L/D ratio in FJB. It is noticed that the Sommerfeld number calculated with the proposed method (PGD) agrees with the results obtained in [34] and from FDM, FDM_{sor} methods.

4.3.3. Friction number

Table 8 shows the variation of the friction number with increasing the eccentricity ratio for different L/D ratio performed using PGD, FDM and FDM_{sor} methods compared with [34].

Table 7
Sommerfeld number for different L/D ratios with different values of the eccentricity ratio.

Parameters		Eccentricity ratio ϵ								
L/D	Sommerfeld	0.1	0.2	0.3	0.4	0.5	0.6	0.7	0.8	0.9
1/4	S-[34]	16.2	7.57	4.49	2.83	1.78	1.07	0.58	0.263	0.0728
	S-PGD	16.24	7.57	4.47	2.81	1.75	1.03	0.55	0.233	0.0566
	S-FDM	17.61	8.24	4.90	3.11	1.97	1.19	0.65	0.299	0.0862
	S-FDM_{sor}	17.61	8.24	4.90	3.11	1.97	1.19	0.65	0.299	0.0861
1/2	S-[34]	4.32	2.03	1.21	0.784	0.508	0.318	0.184	0.0912	0.0309
	S-PGD	4.35	2.038	1.21	0.760	0.480	0.28	0.156	0.0699	0.0202
	S-FDM	4.71	2.23	1.35	0.870	0.570	0.36	0.216	0.1097	0.0383
	S-FDM_{sor}	4.71	2.23	1.35	0.870	0.570	0.36	0.216	0.1097	0.0382
1	S-[34]	1.33	0.631	0.388	0.260	0.178	0.12	0.0776	0.0443	0.0185
	S-PGD	1.38	0.653	0.394	0.255	0.167	0.105	0.0613	0.0299	0.0091
	S-FDM	1.48	0.716	0.446	0.303	0.211	0.145	0.0947	0.0549	0.0233
	S-FDM_{sor}	1.48	0.716	0.446	0.303	0.211	0.145	0.0947	0.0549	0.0233
2	S-[34]	0.559	0.271	0.173	0.122	0.0893	0.0654	0.0463	0.0297	0.0173
	S-PGD	0.638	0.306	0.190	0.128	0.0876	0.0576	0.0342	0.016	0.0059
	S-FDM	0.676	0.33	0.212	0.149	0.1098	0.0806	0.0571	0.0367	0.0178
	S-FDM_{sor}	0.676	0.33	0.212	0.149	0.1098	0.0806	0.0571	0.0367	0.0178

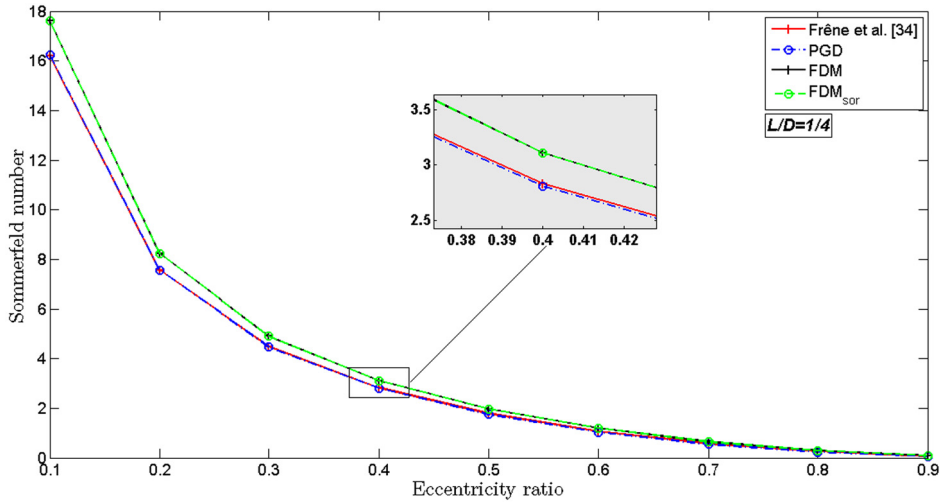

Fig. 22. Sommerfeld number with different values of the eccentricity ratio for FJB ($L/D = 1/4$).

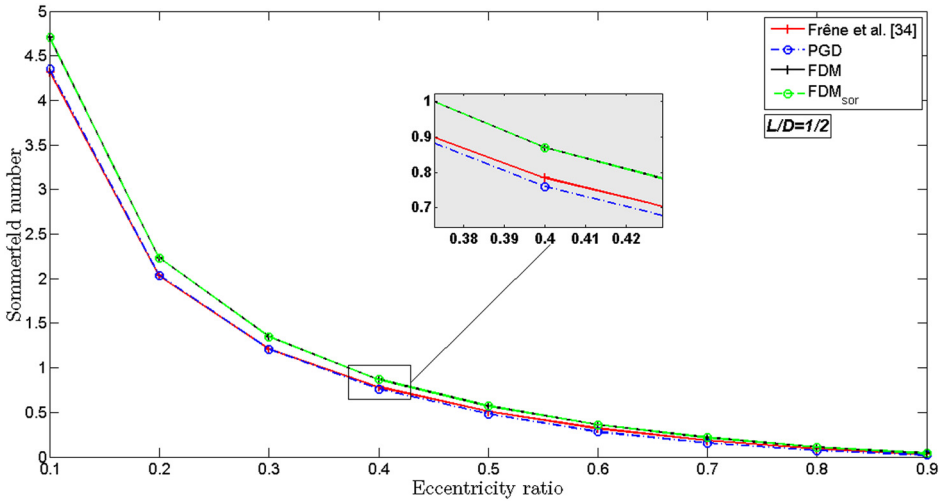

Fig. 23. Sommerfeld number with different values of the eccentricity ratio for FJB ($L/D = 1/2$).

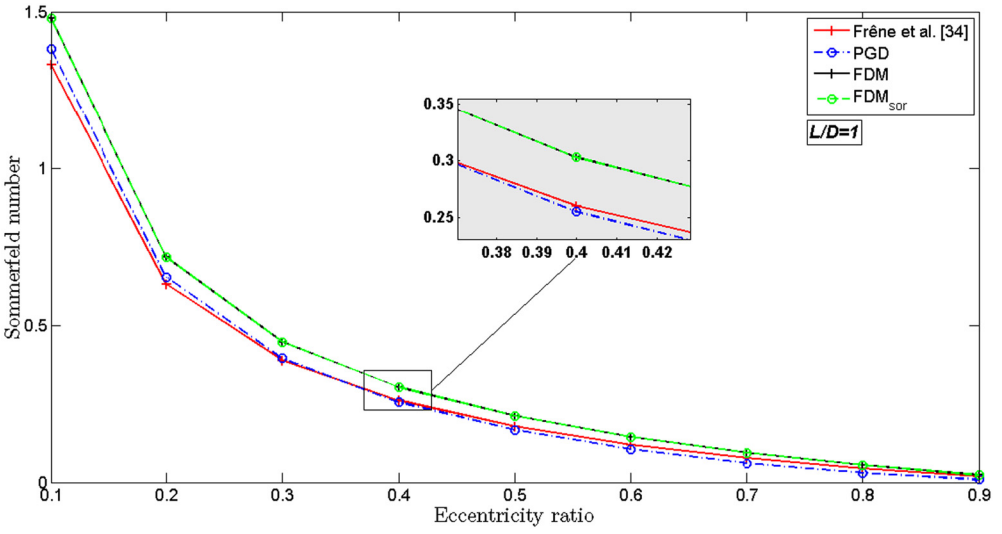

Fig. 24. Sommerfeld number with different values of the eccentricity ratio for FJB ($L/D = 1$).

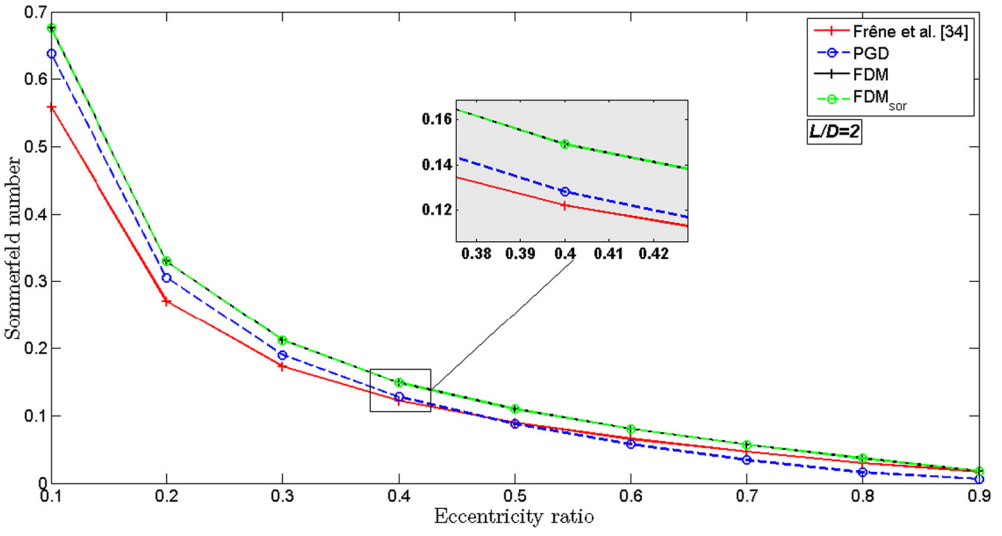

Fig. 25. Sommerfeld number with different values of the eccentricity ratio for FJB ($L/D = 2$).

Figs. 26–29 show the friction number as a function of the eccentricity ratio for different values of the L/D ratio in FJB. It is also noteworthy that there is a very good correspondence between the solution given by PGD and other solutions given by FDM, FDM_{sor} and [34].

Table 8
Friction number for different L/D ratios with different values of eccentricity ratio.

Parameters		Eccentricity ratio ϵ								
L/D	Friction number	0.1	0.2	0.3	0.4	0.5	0.6	0.7	0.8	0.9
1/4	f-[34]	307.0	140.0	82.5	52.67	34.26	21.85	13.19	6.97	2.7
	f-PGD	322.0	152.0	92.6	60.57	40.67	25.64	15.2	7.88	2.56
	f-FDM	349.0	165.0	100.6	65.91	43.67	28.11	16.78	8.53	2.81
	f-FDM_{sor}	349.0	165.0	100.6	65.9	43.66	28.11	16.78	8.53	2.81
1/2	f-[34]	82.1	37.71	22.55	14.75	9.94	6.67	4.33	2.59	1.27
	f-PGD	86.47	41.07	25.05	16.48	10.98	7.13	4.33	2.3	0.91
	f-FDM	93.33	44.35	27.08	17.82	11.85	7.62	4.48	2.12	0.4
	f-FDM_{sor}	93.34	44.37	27.1	17.84	11.88	7.66	4.52	2.16	0.44

(*continued on next page*)

Table 8 (*continued*)

Parameters		Eccentricity ratio ϵ								
L/D	Friction number	0.1	0.2	0.3	0.4	0.5	0.6	0.7	0.8	0.9
1	f-[34]	25.36	11.87	7.35	5.07	3.67	2.7	1.99	1.4	0.859
	f-PGD	27.51	13.17	8.16	5.51	3.81	2.6	1.68	0.98	0.41
	f-FDM	29.26	13.88	8.44	5.49	3.55	2.13	1.02	0.12	0.59
	f-FDM_{sor}	29.28	13.93	8.51	5.59	3.76	2.26	1.17	0.28	0.43
2	f-[34]	10.76	5.21	3.4	2.5	1.96	1.6	1.31	1.04	0.73
	f-PGD	12.67	6.17	3.94	2.76	1.99	1.42	0.94	0.52	0.26
	f-FDM	13.2	6.24	3.75	2.38	1.46	0.74	0.14	0.4	0.9
	f-FDM_{sor}	13.27	6.36	3.94	2.63	1.77	1.11	0.57	0.09	0.38

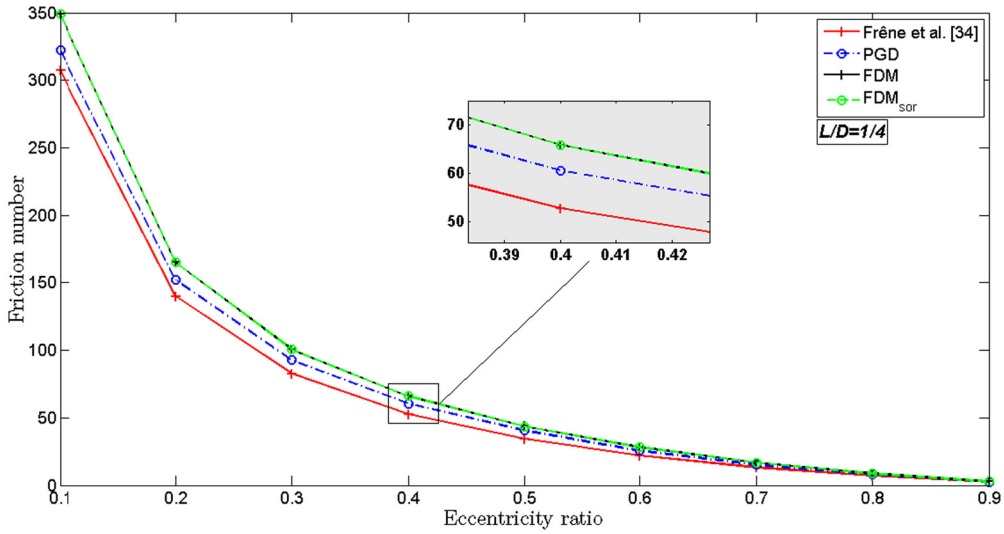

Fig. 26. Friction number with different values of the eccentricity ratio from FJB ($L/D = 1/4$).

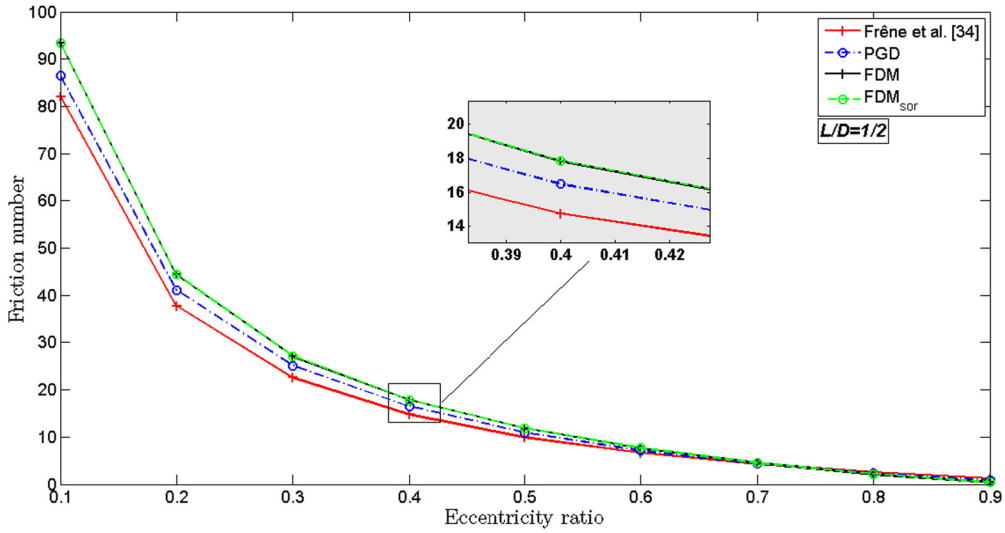

Fig. 27. Friction number with different values of the eccentricity ratio from FJB ($L/D = 1/2$).

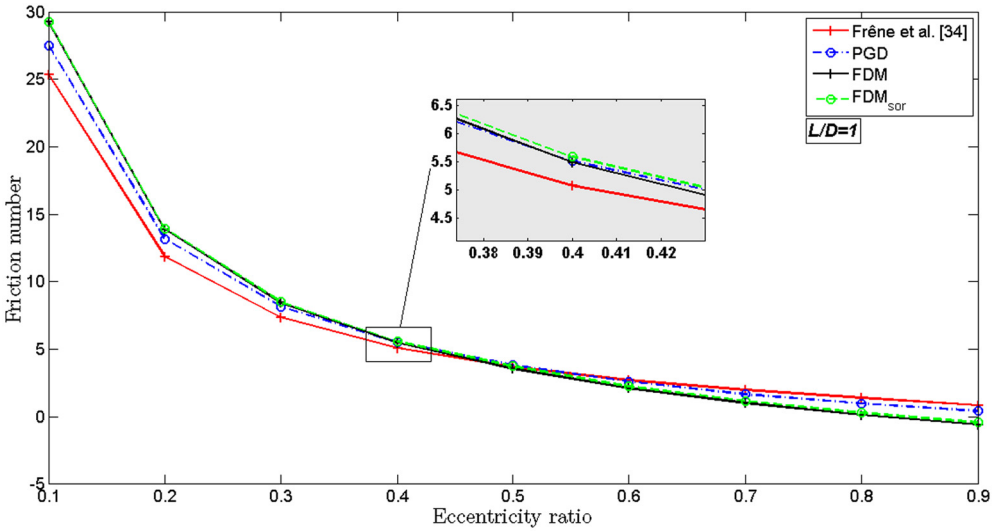

Fig. 28. Friction number with different values of the eccentricity ratio from FJB ($L/D = 1$).

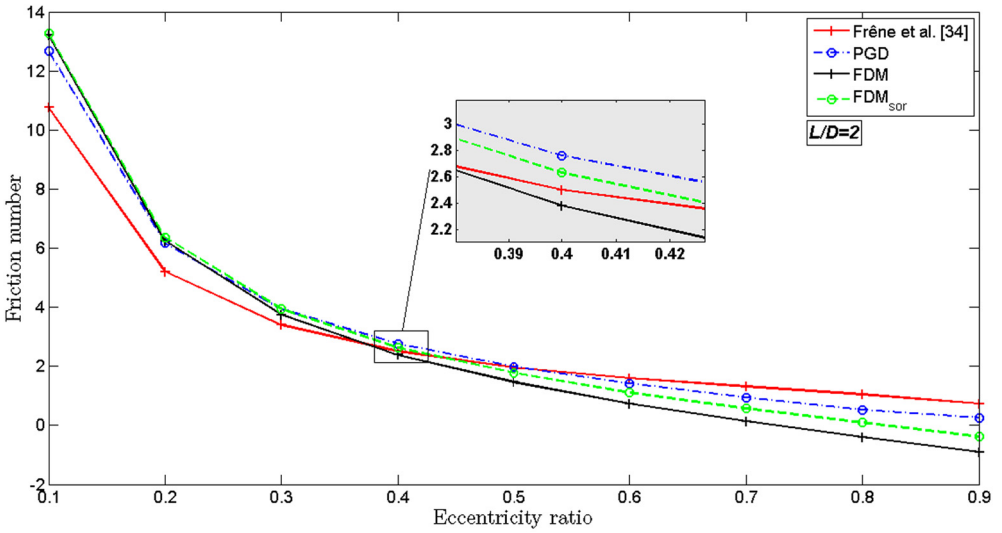

Fig. 29. Friction number with different values of the eccentricity ratio from FJB ($L/D = 2$).

4.3.4. Computational time

The computational time required for the evaluation of the fluid film pressure operating under the following conditions: $L/D = 1$, $\epsilon = 0.1$ and mesh nodes $= [50, 100, 200, ..., 600]^2$, using FDM, FDM$_{sor}$ and PGD methods, is listed in Table 9 and plotted in Fig. 30.

Through this comparison, we notice that the PGD method is clearly more efficient (meaning less time consuming) compared to other methods. But, this time, the number of arithmetic operations required for computation of the solution is investigated. It is observed that the most of the CPU time required by each numerical method (PGD and others) is essentially elasped for solving systems of linear equations. In our case, LU factorization with partial pivoting technique is used for this purpose. The factorization of a square matrix of order N into L and U requires $[(2/3) \cdot N^3]$ floating-point arithmetic op-

Table 9
Comparison of the computational time required for the calculation of the fluid film pressure using FEM, FEM$_{sor}$ and PGD in FJB.

L/D	Method	Mesh (number of nodes)						
		2500	10,000	40,000	90,000	160,000	250,000	360,000
1	PGD	0.11	0.12	0.23	0.54	0.97	1.53	2.33
	FDM	0.15	0.81	21.19	123.57	399.50	985.21	2036.59
	FDM$_{sor}$	0.16	0.87	21.88	126.12	403.23	992.22	2048.64

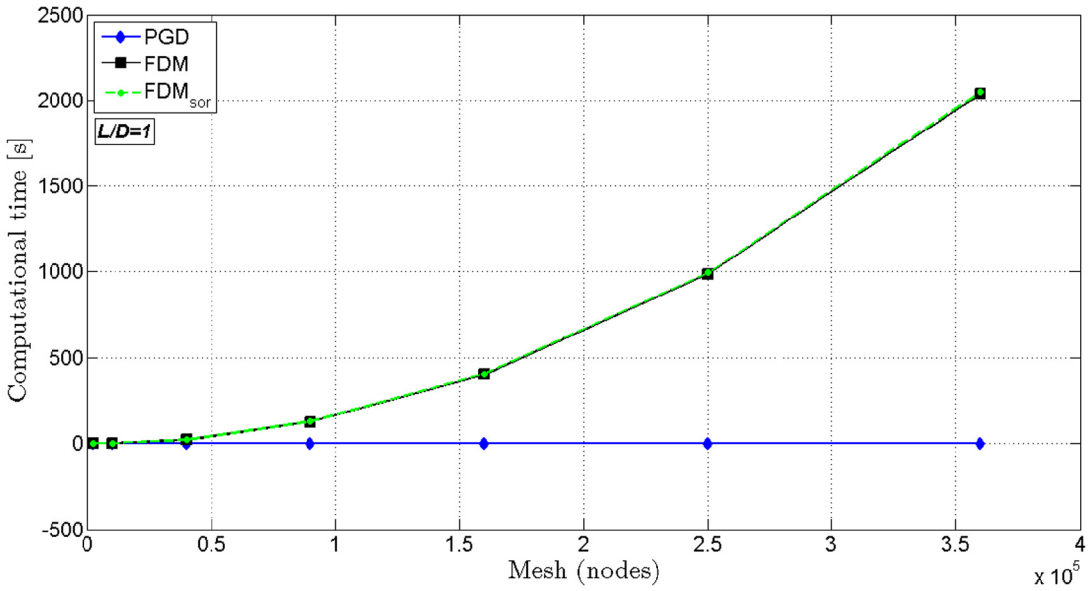

Fig. 30. FDM versus PGD computational time when increasing the number of nodes in FJB.

Table 10
Number of operations for different mesh size from the PGD and FDM methods.

FLOPS	Number of nodes						
	2500	10,000	40,000	90,000	160,000	250,000	360,000
PGD	3.0000e+07	2.4000e+08	1.9200e+09	6.4800e+09	1.5360e+10	3.0000e+10	5.1840e+10
FDM	2.3438e+10	1.5000e+12	9.6000e+13	1.0935e+15	6.1440e+15	2.3438e+16	6.9984e+16

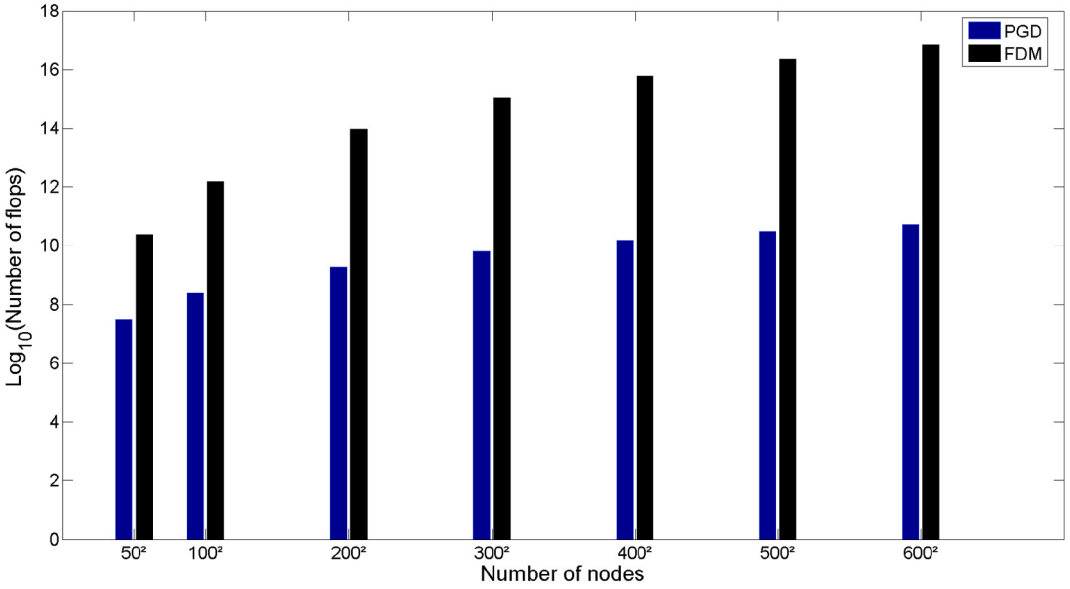

Fig. 31. Number of flops for different mesh configurations.

erations (flops) [37]. Taking into account just flops required for solving linear systems, we can say that in order to solve the resultant system of order $[(N \times N)]$ obtained from FDM we have to consume $[(2/3) \cdot (N \times N)^3]$ flops (for FEM_{SOR} it is even more expensive, in term of flops, due to the additional over-relaxation procedure), whereas, in the PGD method, the space separated representation allows us to reduce the number of flops to $[(2/3) \cdot (N)^3 \cdot number\,of\,dimensions \cdot Max_{\text{terms}} \cdot Max_{\text{fp}}]$ (Algorithm 1), in our case $\text{PGD}_{\text{flops}} = [(2/3) \cdot (N)^3 \cdot 2 \cdot 4 \cdot 20]$. The numbers of flops required for the PGD and FDM methods are listed in Table 10 and plotted in Fig. 31.

From the latter comparison, it is noticed that the number of flops required by PGD is much smaller than that required by FDM, and tends to slightly increase when the number of nodes become prohibitive.

5. Conclusion

In this paper, a new extension of the Proper Generalized Decomposition method for the analysis of journal bearing hydrodynamic lubrication is presented. The main idea of the PGD approach is to compute iteratively each term of the numerical approximation using products of functions defined in lower dimensions, which induces a reduced separated representation of the solution. We have demonstrated that the PGD method is able to solve the Reynolds equation accurately and with impressive CPU time saving, compared to other finite difference models. Another advantage of the proposed approach over other computational methods is to include high accuracy with relatively few grid nodes and an instantaneous solution that is function of the convergence of the fixed point algorithm. In terms of computational time, the verdict is truly impressive: PGD converges at the first node configurations with a relatively constant CPU time, the same error order is attained from FDM methods at a CPU time over thousand times bigger than that of PGD. This work is the first step toward dealing with model order reduction in journal bearing hydrodynamic lubrication. Increasing the order of complexity of this problem to be able to treat a thermo-elasto-hydrodynamic lubrication problem (TEHD) will be the subject of further studies. Indeed, it would be interesting to include other journal bearing model parameters, like the number of grooves and the geometry of sliders as extra-coordinates of the problem. It might be hoped that the real-time resolution property of PGD will be put to profit in real industrial applications.

References

[1] O. Reynolds, On the theory of lubrication and its application to mr. beauchamp tower's experiments, including an experimental determination of the viscosity of olive oil, Proc. R. Soc. Lond. 40 (242–245) (1886) 191–203.
[2] N.P. Petrov, Friction in machines and the effect of the lubricant, Inzherernii Zh. 1 (1883) 71–140.
[3] B. Tower, First report on friction experiments, Proc. Inst. Mech. Eng. 34 (1) (1883) 632–659.
[4] S. Seireg, Friction and Lubrication in Mechanical Design, CRC Press, Boca Raton, 1998.
[5] O. Pinkus, B. Sternlicht, Theory of Hydrodynamic Lubrication, McGraw-Hill, New York, 1961.
[6] G.B. DuBois, F.W. Ocvirk, Analytical Derivation and Experimental Evaluation of Short-Bearing Approximation for Full Journal Bearings, US Government Printing Office, Washington, D.C., USA, 1953.
[7] A.G.M. Michell, Progress in fluid-film lubrication, Trans. Am. Soc. Mech. Eng. 51 (2) (1929) 153–163.
[8] A. Sommerfeld, Zur hydrodynamischen Theorie der Schmiermittelreibung, Z. Math. Phys. 50 (97) (1904) 155.
[9] D. Sfyris, A. Chasalevris, An exact analytical solution of the Reynolds equation for the finite journal bearing lubrication, Tribol. Int. 55 (2012) 46–58.
[10] A. Chasalevris, D. Sfyris, Evaluation of the finite journal bearing characteristics, using the exact analytical solution of the Reynolds equation, Tribol. Int. 57 (2013) 216–234.
[11] A.A. Raimondi, J. Boyd, A solution for the finite journal bearing and its application to analysis and design: I, ASLE Transact. 1 (1) (1958) 159–174.
[12] J.F. Booker, K.H. Huebner, Application of finite element methods to lubrication: an engineering approach, J. Tribol. 94 (4) (1972) 313–323.
[13] M. Deligant, P. Podevin, F. Vidal, W. Tyminski, S. Guilain, H. Lahjaily, 3d thermal steady-state CFD analysis of power friction losses in a turbocharger's journal bearing and comparison with finite difference method and experimentation, in: 12th EAEC, 2009.
[14] P. Liang, C. Lu, J. Ding, S. Chen, A method for measuring the hydrodynamic effect on the bearing land, Tribol. Int. 67 (2013) 146–153.
[15] V.K. Dwivedi, S. Chand, K.N. Pandey, Effect of number and size of recess on the performance of hybrid (hydrostatic/hydrodynamic) journal bearing, Proc. Eng. 51 (2013) 810–817.
[16] N. Raghavendra, M.C. Math, P.R. Sharma, Finite element method analysis of hydrodynamic journal bearing, Eur. J. Adv. Eng. Technology. 2 (2) (2015) 92–101.
[17] M.F. Barone, I. Kalashnikova, M.R. Brake, D.J. Segalman, Reduced order modeling of fluid/structure interaction, Sandia National Laboratories Report, SAND No. 7189, 2009.
[18] W.H.A. Schilders, H.A. Van der Vorst, J. Rommes, Model Order Reduction: Theory, Research Aspects and Applications, vol. 13, Springer, 2008.
[19] Z.-Q. Qu, Model Order Reduction Techniques with Applications in Finite Element Analysis, Springer Science & Business, Media, 2013.
[20] G. Berkooz, P. Holmes, J.L. Lumley, The proper orthogonal decomposition in the analysis of turbulent flows, Annu. Rev. Fluid Mech. 25 (1) (1993) 539–575.
[21] C. Leblond, C. Allery, C. Inard, An optimal projection method for the reduced-order modeling of incompressible flows, Comput. Methods Appl. Mech. Eng. 200 (33) (2011) 2507–2527.
[22] N. Akkari, A. Hamdouni, E. Liberge, M. Jazar, A mathematical and numerical study of the sensitivity of a reduced order model by pod (rom–pod), for a 2d incompressible fluid flow, J. Comput. Appl. Math. 270 (2014) 522–530.
[23] P. Ladeveze, Nonlinear Computational Structural Mechanics, 1999.
[24] A. Nouy, P. Ladevèze, Multiscale computational strategy with time and space homogenization: a radial-type approximation technique for solving microproblems, Int. J. Multiscale Comput. Eng. 2 (4) (2004).
[25] P. Ladeveze, J.-C. Passieux, D. Néron, The Latin multiscale computational method and the proper generalized decomposition, Comput. Methods Appl. Mech. Eng. 199 (21) (2010) 1287–1296.
[26] F. Chinesta, P. Ladevèze, E. Cueto, A short review on model order reduction based on proper generalized decomposition, Arch. Comput. Methods Eng. 18 (4) (2011) 395–404.
[27] A. Ammar, B. Mokdad, F. Chinesta, R. Keunings, A new family of solvers for some classes of multidimensional partial differential equations encountered in kinetic theory modeling of complex fluids, J. Non-Newton. Fluid Mech. 139 (3) (2006) 153–176.
[28] A. Ammar, B. Mokdad, F. Chinesta, R. Keunings, A new family of solvers for some classes of multidimensional partial differential equations encountered in kinetic theory modelling of complex fluids: part II: transient simulation using space-time separated representations, J. Non-Newton. Fluid Mech. 144 (2) (2007) 98–121.
[29] B. Mokdad, E. Prulière, A. Ammar, F. Chinesta, On the simulation of kinetic theory models of complex fluids using the Fokker–Planck approach, Appl. Rheol. 17 (2) (2007) 26494.
[30] A. Dumon, C. Allery, A. Ammar, Proper general decomposition (pgd) for the resolution of Navier–Stokes equations, J. Comput. Phys. 230 (4) (2011) 1387–1407.

[31] A. Dumon, C. Allery, A. Ammar, Proper generalized decomposition method for incompressible Navier–Stokes equations with a spectral discretization, Appl. Math. Comput. 219 (15) (2013) 8145–8162.
[32] M.S. Aghighi, A. Ammar, C. Metivier, M. Normandin, F. Chinesta, Non-incremental transient solution of the Rayleigh–Bénard convection model by using the pgd, J. Non-Newton. Fluid Mech. 200 (2013) 65–78.
[33] L. Tamellini, O. Le Maitre, A. Nouy, Model reduction based on proper generalized decomposition for the stochastic steady incompressible Navier–Stokes equations, SIAM J. Sci. Comput. 36 (3) (2014) A1089–A1117.
[34] J. Frêne, D. Nicolas, B. Degueurce, D. Berthe, M. Godet, Hydrodynamic Lubrication: Bearings and Thrust Bearings, vol. 33, Elsevier, 1997.
[35] D.M. Smith, Journal Bearings in Turbomachinery, Springer Science & Business Media, 2013.
[36] M. Born, Arnold Johannes Wilhelm Sommerfeld. 1868–1951, in: Obituary Notices of Fellows of the Royal Society, 1952, pp. 275–296.
[37] J. Dongarra, K. Madsen, J. Wasniewski, Applied Parallel Computing: State of the Art in Scientific Computing, vol. 3732, Springer Science & Business Media, 2006.